Ultra-Compact Concurrent Multi-Directional Beamforming Receiving Network for High-Efficiency Wireless Power Transfer (WPT)

A Thesis
Presented to
The Academic Faculty

by

Min-Yu Huang

In Partial Fulfillment
of the Requirements for the Degree
Masters in the
School of Electrical and Computer Engineering

Georgia Institute of Technology
December 2018

Ultra-Compact Concurrent Multi-Directional Beamforming Receiving Network for High-Efficiency Wireless Power Transfer (WPT)

Approved by:

Dr. Madhavan Swaminathan
School of Electrical and Computer Engineering
Georgia Institute of Technology

Dr. Gee-Kung Chang
School of Electrical and Computer Engineering
Georgia Institute of Technology

Dr. Hua Wang, Advisor
School of Electrical and Computer Engineering
Georgia Institute of Technology

Date Approved: 12/7/2018

TABLE OF CONTENTS

	Page
LIST OF TABLES	iv
LIST OF FIGURES	v
SUMMARY	vii
CHAPTER	
1 INTRODUCTION	1
2 1×4 ARRAY-BASED HIGH-EFFICIENCY RECTENNA ARRAY	5
A. Discussion for field-of-view operation	5
B. Theoretical derivation and analysis for field-of-view operation	9
C. Ultra-compact 4×4 Butler matrix design	14
D. High-efficiency rectifier design	22
E. Wideband end-fire bow-tie antenna design	24
5 MEASUREMENT RESULTS	26
6 CONCLUSION	32
REFERENCES	34

LIST OF TABLES

Page

Table 1. Comparison of state-of-the-art 33

LIST OF FIGURES

Page

Figure 1. WPT for future self-powered applications 1

Figure 2. conventional rectenna array design [10] 2

Figure 3. Proposed multi-direction array-based high-efficiency WPT rectenna array 3

Figure 4. Conventional WPT rectenna array 5

Figure 5. Simple power-combined WPT rectenna array 6

Figure 6. Proposed array-based high-efficiency WPT rectenna array 7

Figure 7. Comparison of the three WPT rectenna array 8

Figure 8. simplified schematic of the proposed rectenna array 9

Figure 9. Ideal coupled-line based 4×4 Butler matrix schematic of the proposed rectenna array 13

Figure 10. Simulated S-parameter for the ideal Butler matrix schematic of the proposed rectenna array 13

Figure 11. Simulated receiving DC power of the proposed 1×4 rectenna array 14

Figure 12. Schematic of the proposed 4×4 Butler matrix 14

Figure 13. The (a) transformer-based quadrature hybrid schematic and (b) its even-mode half-circuit and (c) odd-mode half-circuit. 16

Figure 14. 4-layer FR4-Rogers hybrid PCB stack-up 19

Figure 15. 3D EM HFSS of the 45˚ phase shifter and the proposed 4×4 Butler matrix 20

Figure 16. Measured amplitude performance of the proposed 4×4 Butler matrix 21

Figure 17. A 3-stage Dickson voltage doubler design example and its 3D EM HFSS model 22

Figure 18. A high-efficiency rectifier design example and its 3D EM HFSS model 24

Figure 19. A 1×4 bow-tie end-fire antenna array design example and its 3D EM HFSS model 25

Figure 20. A fabricated high-efficiency rectifier sample 26

Figure 21. Measured RF-to-DC efficiency versus the RF Pin 26

Figure 22. A fabricated concurrent multi-direction array-based high-efficiency WPT sample 27

Figure 23. Measurement setup for the synthesized phased array generation and the rectenna array characterization 28

Figure 24. Measured normalized DC power for proposed WPT and conventional design 29

Figure 25. Measured input matching for each input of the 1×4 antenna array 30

Figure 26. Far-field measurement setup 30

Figure 27. Measured normalized DC power for proposed WPT and conventional design in far-field 31

SUMMARY

This thesis demonstrates an all-passive ultra-compact low-loss array-based beamforming rectenna array for high-efficiency wireless power transfer (WPT). The detailed circuit analysis and theoretical derivation are presented in the paper, showing that the proposed circuit can achieve full field-of-view (FoV) WPT operation with scalable array-based RF-to-DC efficiency improvement. A proof-of-concept 4-element rectenna design example at 2.4GHz is implemented in a 4-layer FR4-Rogers hybrid PCB. The compact transformer-based 4×4 Butler matrix design with at least 100× size reduction as the passive beamformer is implemented in the WPT design for supporting concurrent multi-direction beam reception. At 2.4GHz, measurement for the Butler matrix exhibits an insertion loss of 0.8dB, a return loss better than 10dB (DC-3GHz), and a peak-to-null ratio > 35dB. Then, with the proposed passive beamformer, the measurement results of the proposed WPT network achieves at least full-FoV 2.4× and a peak 3× RF-to-DC efficiency enhancement compared to conventional rectenna array design. To the best of our knowledge, this is the first complete analysis and demonstration of a compact scalable N-element array-based beamforming rectenna array network for full-FoV high-efficiency WPT.

CHAPTER I

INTRODUCTION

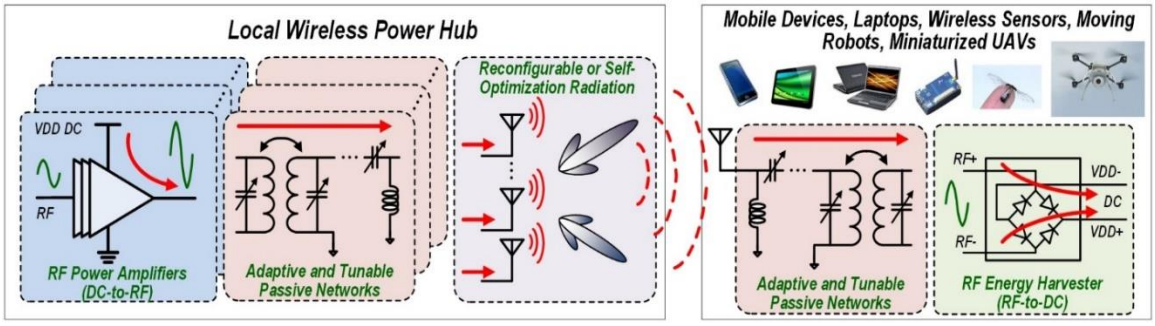

Figure 1. WPT for future self-powered applications

Wireless power transfer (WPT) ([1]-[14],[23][24]) has been rapidly developing in several applications including microwave powered aircraft / solar powered satellites, radio frequency identification (RFID), and the fast-growing Internet of Things (IoT). Moreover, future complex EM environments will require multiple compact sensors and devices which dynamically interact to communicate and deliver numerous data streams, necessitating energy-efficient and low-latency systems [15]-[18]. The RF WPT can serve as a potential candidate for self-powering/-driving these devices in future versatile applications. Conventional energy harvesting networks have been studied via inductive or resonant near-field powering [1], far-field directive power beaming [2]–[5], and nondirective low-power far-field harvesting [6]–[9]. However, none of them support long-range power transfer for the future sensor networking. Recently, [10]-[14] proposed far-field power harvesters with low incident power densities in the long range by using arrays of antennas integrated with rectifiers and power-management circuits (Fig. 2). The rectenna array is applied to simply accumulate and sum the output DC power, generating sufficient total output DC power to drive the other devices in the self-powered system. The overall rectification DC power can be expressed as

$$P_{DC,\,Conventional} \sim N \times \eta_1 \times P_{pixel}, \quad (1)$$

where N is the number of the elements of the antenna array, η_1 is the rectification efficiency of the rectifiers, and P_{pixel} is the antenna gain of each pixel.

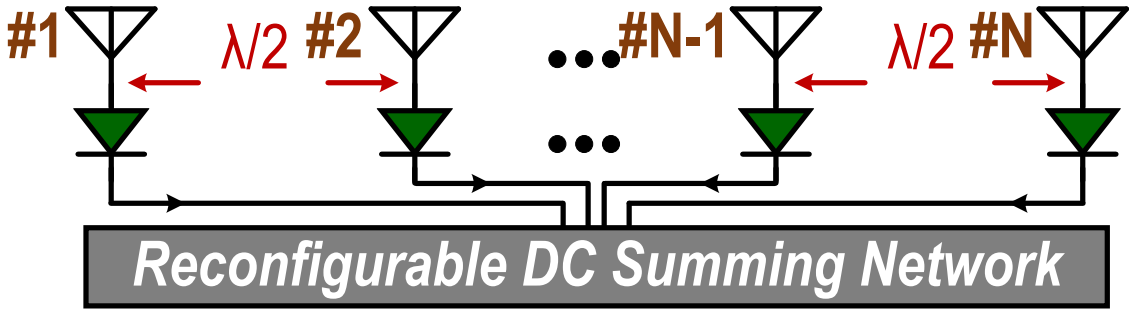

Figure 2. conventional rectenna array design [10]

For the conventional rectenna array, although a large-scale array size is applied, there is no array factor enhancement for the design since the incoming RF signals are not beam-formed before the rectifiers. Moreover, for each element, the signal injected to the rectifier operates with a low rectification efficiency due to the low RF signal swing before the rectifiers. The conventional rectenna array may not support multi-direction/-beam reception due to direct signal summation at the antenna node. For example, in an extreme case, if there are two out-of-phase signals injected to the array, the RF signals directly sum and cancel out each other at the input of the rectifiers, showing that the conventional rectenna array is not capable of processing multiple RF signals simultaneously.

To address these challenges, this paper proposes an all-passive beam-formed array-based high-efficiency WPT to support dynamic, full FoV, and multi-beam far-field energy harvesting. Compared to the conventional rectenna designs, the proposed circuit adds an extra N×N Butler matrix to process multi-directional signals concurrently and provide passive beamforming with an array factor for RF signal enhancement (Fig. 3). The overall rectification DC power is

$$P_{DC,\ proposed} \sim N \times N \times \eta_2 \times P_{pixel}, \quad (2)$$

where the N is the element number of the antenna array, η_2 is the rectification efficiency of the rectifiers, and P_{pixel} is the antenna gain of each pixel.

Compared to (1), it shows that there is a factor of N times larger improvement since the passive N×N Butler matrix beam-forms signals with an array factor enhancement before the rectifier. Also, the input signal swing seen by the following rectifiers would be larger. Thus, the rectification efficiency η_2 in (2) would be larger than the η_1 in (1). Furthermore, the N×N Butler matrix beamformer is built by multiple passive couplers with various fixed phase-shifts, supporting concurrent multi-direction beamforming/-tracing. Note that the proposed structure is fully passive, ensuring that the DC output power is fully utilized for the self-powered system.

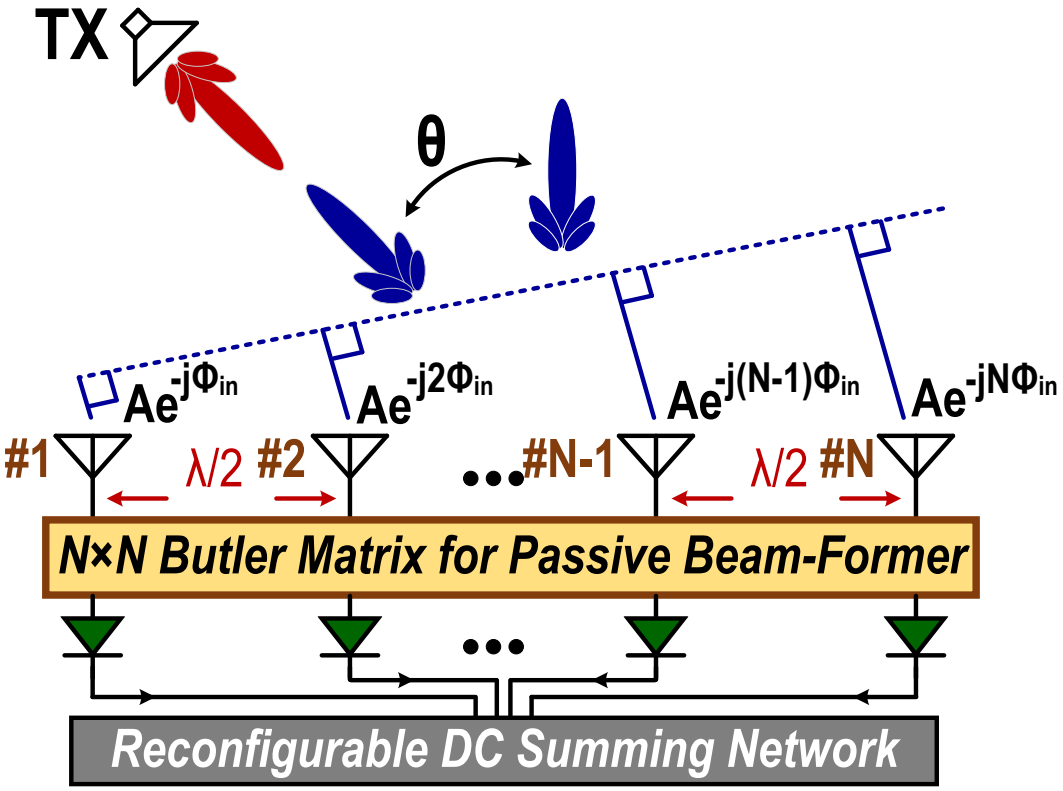

Figure 3. Proposed multi-direction array-based high-efficiency WPT rectenna array

A proof-of-concept 1×4 rectenna design at 2.4GHz shows that it can achieve at least 2.4× larger received RF power compared to the conventional design over full FoV. The 4×4 Butler matrix is made in hybrid passive structure designs by fusing lumped elements (transformers, inductors, capacitors) and distributed elements, achieving 100× size reduction compared to conventional Butler matrix designs.

This thesis is organized as follows. Chapter 2 will show the detailed schematic and theorical derivation for the proposed multi-direction concurrent array-based high-efficiency WPT design. In Chapter3, it shows the measurement results for the proof-of-concept design example. Chapter 4 will summarize and conclude the design with a comparison table to state-of-the-art designs.

CHAPTER II

1×4 ARRAY-BASED HIGH-EFFICIENCY RECTENNA ARRAY

A. Discussion for field-of-view operation

Three different scenarios for designing the rectenna array are first analyzed (Fig.4 - Fig.6). In the Fig. 4, it shows mentioned conventional rectenna array design. It can achieve full field-of-view coverage since the phase information of the incoming signals are rectified out due to the square-law rectifier device. Thus, DC power of each outputs includes no phase-dependent information and can be directly summed together. The operation is not related any beam-forming and no array factor improvement here. There is no extra passive structure inserted between the antenna array and the rectifier array, showing that there is no extra passive loss for degrading the incoming RF signal swing for the following rectifiers.

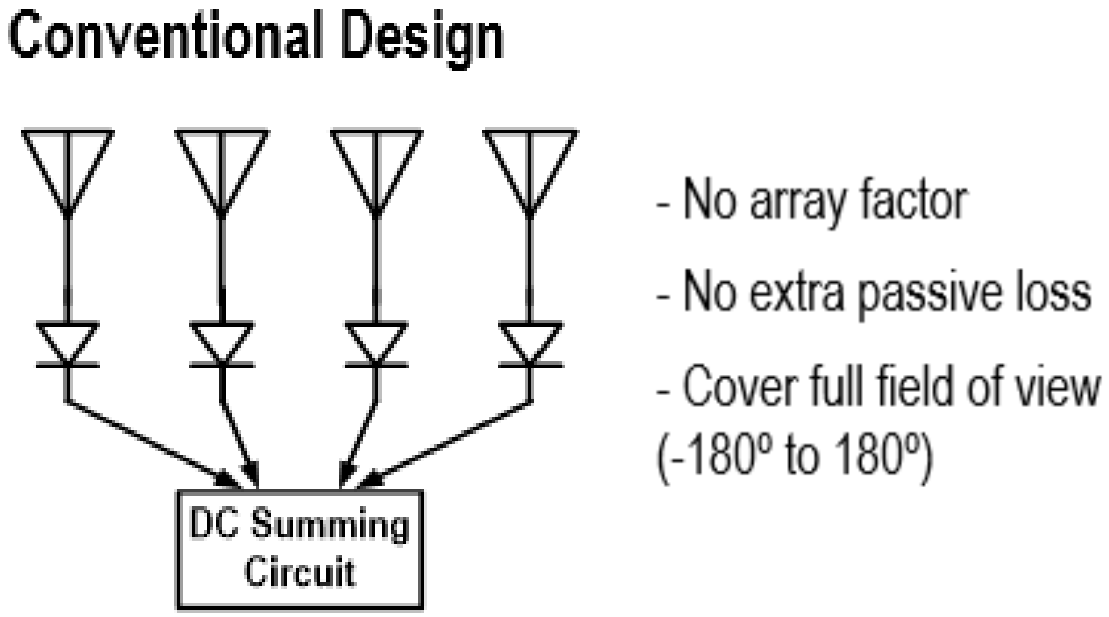

Figure 4. Conventional WPT rectenna array

On the other hand, one can use a simple 4-to-1 power combiner to directly add the 4 incoming RF signals between the antenna array and the rectifier array to increase the RF signal swing for the rectifiers (Fig. 5). However, the RF signals with array factor enhancement only happen at input progressive phase shifts ϕin = 0˚. In a uniform 1×4 array, the input progressive phase shifts are ϕin, 2ϕin, 3ϕin, 4ϕin for the adjacent 4 paths. For some extreme cases, the RF signals are fully canceled to each other as they are input progressive phase shifts ϕin = 90˚ and 180˚. The RF signals form an array factor null and then generate zero rectified DC output power. This issue would be even severe when the array size is scaled to a larger-element phased array which the beamforming coverage and field-of-view would be much narrower. In summary, although the technique provides an array factor enhancement near boresight incident angle (ϕin = 0˚), the field-of-view is limited. Here, the 2-stage Wilkinson power combiner is applied to serve as the power combiner example with a reasonable 2dB extra passive loss.

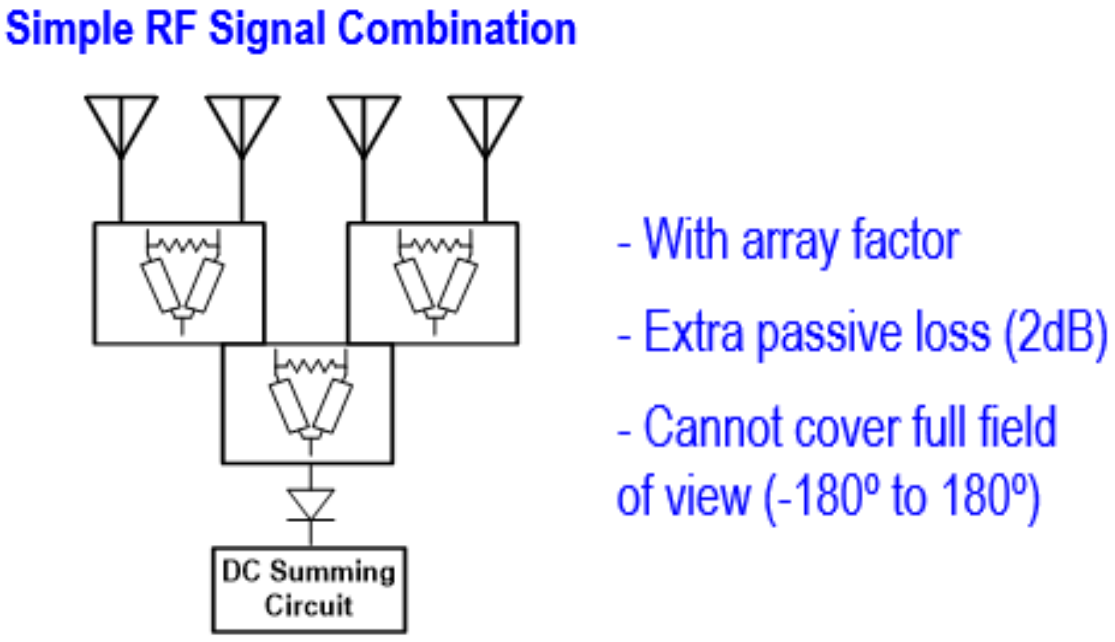

Figure 5. Simple power-combined WPT rectenna array

As for the proposed design (Fig. 6), although it includes extra passive loss of the 4×4 Butler matrix, it preserves a full field-of-view operation with an array factor enhancement (detailed analysis is shown in Chapter II-B). It will be robust to any progressive phase shifts for the incoming RF signals and beamformed RF signal would drive the following rectifier array with higher rectification efficiency. Moreover, it is the one which can support concurrent multi-direction RF signal process. Assume there is also 2 dB passive loss of the proposed passive beam-former, comparison of the three designs are simulated via mathematic derivation and shown in the Fig. 7.

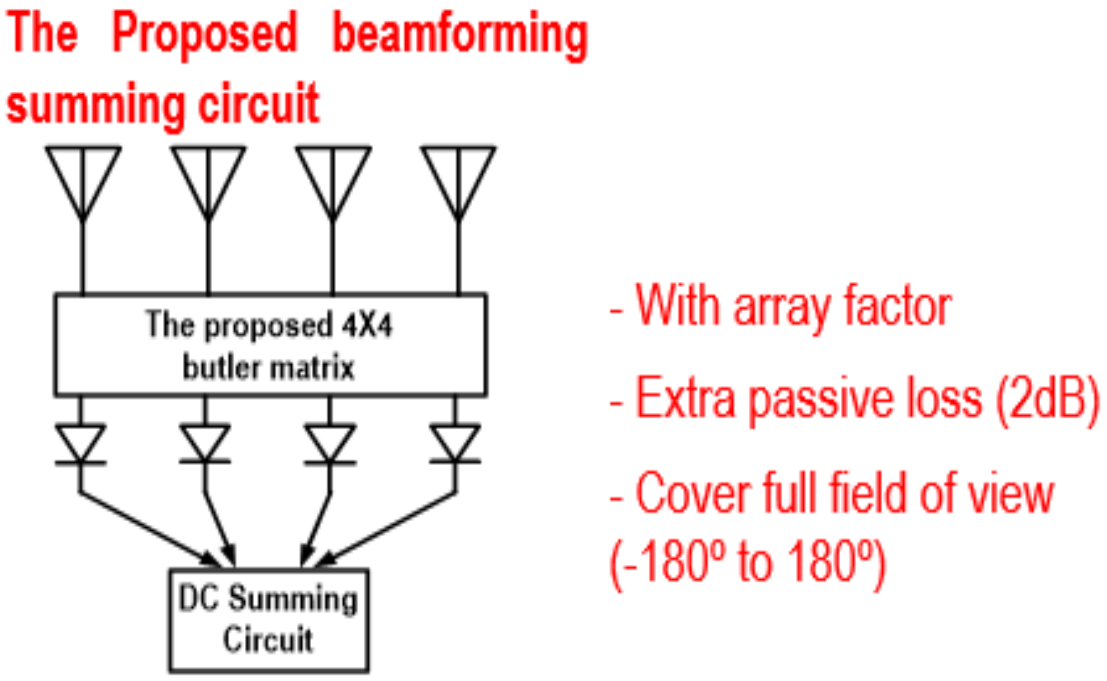

Figure 6. Proposed array-based high-efficiency WPT rectenna array

Based on the equation (2), it shows that the proposed design can serve at least 4× receiving power improvement, which is 10log4 = 6dB enhancement for a 1×4 array. With the consideration of the 2dB extra passive loss, it still preserves 4dB receiving power improvement. Compared to the conventional design, both are with a full-field-of-view coverage, but the proposed design serves at least 2.5× rectified output DC power (Fig. 7).

On the other hand, although the proposed circuit is with same rectified power enhancement to the simple power-combined WPT rectenna array, it preserves full field-of-view power enhancement even at end-fire incidence. Here, the rectified efficiency applied for the three cases are assumed that they are with same value; however, in reality, the proposed design would serve highest RF-to-DC efficiency for the rectifier array due to full field-of-view array factor enhancement as well as a large driving RF signals in front of the rectifiers.

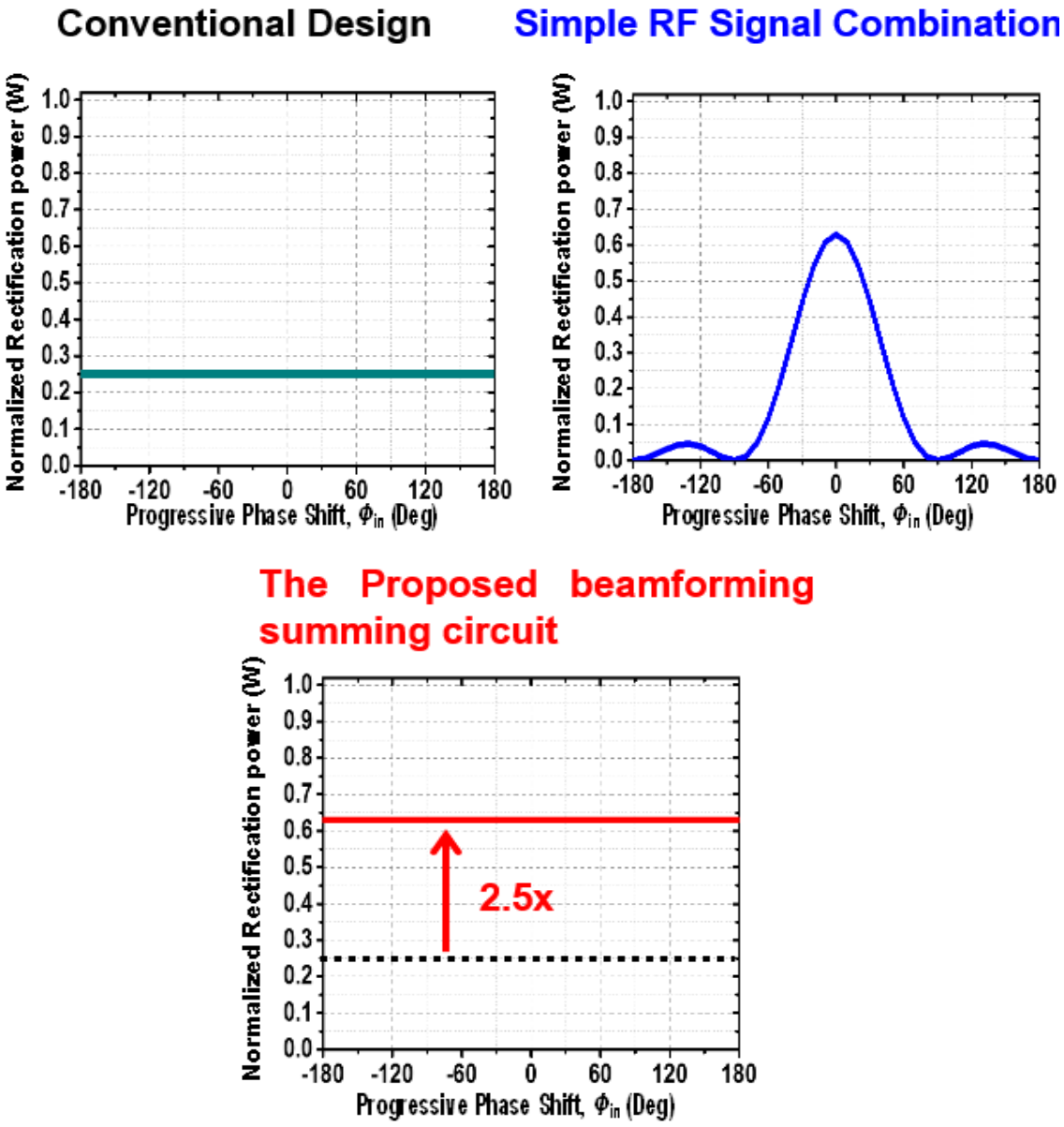

Figure 7. Comparison of the three WPT rectenna array

B. Theoretical derivation and analysis for field-of-view operation

The figure 8 shows the simplified schematic proposed array-based beam-formed 1×4 rectenna array for high-efficiency WPT. Assuming there is input progress phase shift ϕin for the adjacent channel injected the proposed passive beam-former 4×4 Butler matrix, each input and output for 4 followed rectifier R1~R4 are analyzed and derived first.

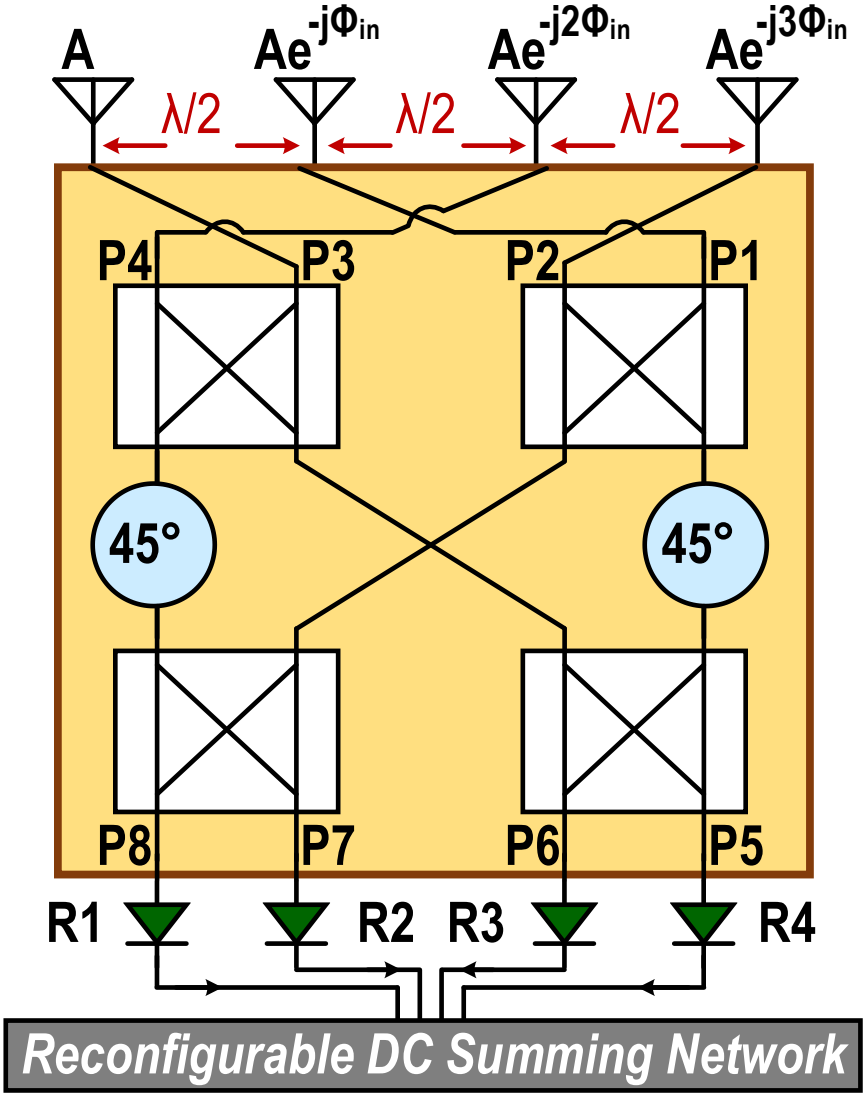

Figure 8. simplified schematic of the proposed rectenna array

At the input of R1, the four incoming RF signals are phase shifted and combined by the 4×4 Butler matrix with an amplitude loss α. The combined RF signal at the R1 input can be expressed as

$$\alpha A_{in}[e^{j\left(\frac{\pi}{4}\right)} + e^{j(-\phi\text{in}+\pi)} + e^{j\left(-2\phi\text{in}-\frac{\pi}{4}\right)} + e^{j\left(-3\phi\text{in}+\frac{\pi}{2}\right)}] \quad (3)$$

Since the rectifier is square-law device, the combined RF signal (3) after the rectification of the R1, i.e. output of the R1, is

$$\alpha^2 {A_{in}}^2 \left|e^{j(-\phi\text{in})} * \left[e^{j\left(\phi\text{in}+\frac{\pi}{4}\right)} + e^{j(\pi)} + e^{j\left(-\phi\text{in}-\frac{\pi}{4}\right)} + e^{j\left(-2\phi\text{in}+\frac{\pi}{2}\right)}\right]\right|^2$$

$$= \alpha^2 {A_{in}}^2 \left|2\cos\left(\phi\text{in}+\frac{\pi}{4}\right) - 1 + \sin(2\phi\text{in}) + j\cos(2\phi\text{in})\right|^2$$

$$= \alpha^2 {A_{in}}^2 [4\cos^2\left(\phi\text{in}+\frac{\pi}{4}\right) + 2\cos\left(\phi\text{in}+\frac{\pi}{4}\right)\sin(2\phi\text{in}) + \sin^2(2\phi\text{in})$$

$$-4\cos\left(\phi\text{in}+\frac{\pi}{4}\right) - 2\sin(2\phi\text{in}) + 1 + \cos^2(2\phi\text{in})]$$

$$= \alpha^2 {A_{in}}^2 \{4\cos\left(\phi\text{in}+\frac{\pi}{4}\right)[\cos\left(\phi\text{in}+\frac{\pi}{4}\right) + \sin(2\phi\text{in}) - 1] - 2\sin(2\phi\text{in}) + 2\} \quad (4)$$

The similar derivation can be applied to the R2. The combined RF signal before the R2 can be expressed as

$$\alpha A_{in}[e^{j\left(\frac{3\pi}{4}\right)} + e^{j\left(-\phi\text{in}+\frac{\pi}{2}\right)} + e^{j\left(-2\phi\text{in}+\frac{\pi}{4}\right)} + e^{j(-3\phi\text{in})}] \quad (5)$$

Then, the combined RF signal (5) after the rectification of the R2 is

$$\alpha^2 {A_{in}}^2 \left|e^{j\left(-\phi\text{in}+\frac{\pi}{2}\right)} * \left[e^{j\left(\phi\text{in}+\frac{\pi}{4}\right)} + 1 + e^{j\left(-\phi\text{in}-\frac{\pi}{4}\right)} + e^{j\left(-2\phi\text{in}-\frac{\pi}{2}\right)}\right]\right|^2$$

$$= \alpha^2 {A_{in}}^2 \left|2\cos\left(\phi\text{in}+\frac{\pi}{4}\right) + 1 - \sin(2\phi\text{in}) + j\cos(2\phi\text{in})\right|^2$$

$$= \alpha^2 {A_{in}}^2 [4\cos^2\left(\phi\text{in}+\frac{\pi}{4}\right) - 2\cos\left(\phi\text{in}+\frac{\pi}{4}\right)\sin(2\phi\text{in}) + \sin^2(2\phi\text{in})$$

$$+4\cos\left(\phi\text{in}+\frac{\pi}{4}\right) - 2\sin(2\phi\text{in}) + 1 + \cos^2(2\phi\text{in})]$$

$$= \alpha^2 {A_{in}}^2 \{4\cos\left(\phi\text{in}+\frac{\pi}{4}\right)[\cos\left(\phi\text{in}+\frac{\pi}{4}\right) - \sin(2\phi\text{in}) + 1] - 2\sin(2\phi\text{in}) + 2\} \quad (6)$$

For the R3. The combined RF signal before the R3 can be expressed as

$$\alpha A_{in}[1 + e^{j\left(-\phi\text{in}+\frac{\pi}{4}\right)} + e^{j\left(-2\phi\text{in}+\frac{\pi}{2}\right)} + e^{j\left(-3\phi\text{in}+\frac{3\pi}{4}\right)}] \quad (7)$$

Then, the combined RF signal (5) after the rectification of the R3 is

$$\alpha^2 {A_{in}}^2 \left|e^{j\left(-\phi\text{in}+\frac{\pi}{4}\right)} * \left[e^{j\left(\phi\text{in}-\frac{\pi}{4}\right)} + 1 + e^{j\left(-\phi\text{in}+\frac{\pi}{4}\right)} + e^{j\left(-2\phi\text{in}+\frac{\pi}{2}\right)}\right]\right|^2$$

$$= \alpha^2 {A_{in}}^2 \left|2\cos\left(\phi\text{in} - \frac{\pi}{4}\right) + 1 + \sin(2\phi\text{in}) + j\cos(2\phi\text{in})\right|^2$$

$$= \alpha^2 {A_{in}}^2 [4\cos^2\left(\phi\text{in} - \frac{\pi}{4}\right) + 2\cos\left(\phi\text{in} + \frac{\pi}{4}\right)\sin(2\phi\text{in}) + \sin^2(2\phi\text{in})$$

$$+4\cos\left(\phi\text{in} - \frac{\pi}{4}\right) + 2\sin(2\phi\text{in}) + 1 + \cos^2(2\phi\text{in})]$$

$$= \alpha^2 {A_{in}}^2 \{4\cos\left(\phi\text{in} - \frac{\pi}{4}\right)[\cos\left(\phi\text{in} - \frac{\pi}{4}\right) + \sin(2\phi\text{in}) + 1] + 2\sin(2\phi\text{in}) + 2\} \quad (8)$$

For the R4. The combined RF signal before the R4 can be expressed as

$$\alpha A_{in}[e^{j\left(\frac{\pi}{2}\right)} + e^{j\left(-\phi\text{in}-\frac{\pi}{4}\right)} + e^{j(-2\phi\text{in}+\pi)} + e^{j\left(-3\phi\text{in}+\frac{\pi}{4}\right)}] \quad (9)$$

Then, the combined RF signal (5) after the rectification of the R3 is

$$\alpha^2 {A_{in}}^2 \left|e^{j\left(-\phi\text{in}+\frac{3\pi}{4}\right)} * \left[e^{j\left(\phi\text{in}-\frac{\pi}{4}\right)} + e^{j(-\pi)} + e^{j\left(-\phi\text{in}+\frac{\pi}{4}\right)} + e^{j\left(-2\phi\text{in}-\frac{\pi}{2}\right)}\right]\right|^2$$

$$= \alpha^2 {A_{in}}^2 \left|2\cos\left(\phi\text{in} - \frac{\pi}{4}\right) - 1 - \sin(2\phi\text{in}) - j\cos(2\phi\text{in})\right|^2$$

$$= \alpha^2 {A_{in}}^2 [4\cos^2\left(\phi\text{in} - \frac{\pi}{4}\right) - 2\cos\left(\phi\text{in} + \frac{\pi}{4}\right)\sin(2\phi\text{in}) + \sin^2(2\phi\text{in})$$

$$-4\cos\left(\phi\text{in} - \frac{\pi}{4}\right) + 2\sin(2\phi\text{in}) + 1 + \cos^2(2\phi\text{in})]$$

$$= \alpha^2 {A_{in}}^2 \{4\cos\left(\phi\text{in} - \frac{\pi}{4}\right)[\cos\left(\phi\text{in} - \frac{\pi}{4}\right) - \sin(2\phi\text{in}) - 1] + 2\sin(2\phi\text{in}) + 2\} \quad (10)$$

Based on the derivation from (3)-(10), the 4 rectified DC outputs (4), (6), (8), (10) are then summed by the DC combiner, the overall DC output power is

$$\alpha^2 {A_{in}}^2\{4\cos\left(\phi\text{in}+\frac{\pi}{4}\right)[\cos\left(\phi\text{in}+\frac{\pi}{4}\right)+\sin(2\phi\text{in})-1]-2\sin(2\phi\text{in})+2\}$$

$$+\quad \alpha^2 {A_{in}}^2\{4\cos\left(\phi\text{in}+\frac{\pi}{4}\right)[\cos\left(\phi\text{in}+\frac{\pi}{4}\right)-\sin(2\phi\text{in})+1]-2\sin(2\phi\text{in})+2\}$$

$$+\quad \alpha^2 {A_{in}}^2\{4\cos\left(\phi\text{in}-\frac{\pi}{4}\right)[\cos\left(\phi\text{in}-\frac{\pi}{4}\right)+\sin(2\phi\text{in})+1]+2\sin(2\phi\text{in})+2\}$$

$$+\quad \alpha^2 {A_{in}}^2\{4\cos\left(\phi\text{in}-\frac{\pi}{4}\right)[\cos\left(\phi\text{in}-\frac{\pi}{4}\right)-\sin(2\phi\text{in})-1]+2\sin(2\phi\text{in})+2\}$$

$$= 8\ \alpha^2 {A_{in}}^2\cos^2\{\left(\phi\text{in}+\frac{\pi}{4}\right)+\cos^2\left(\phi\text{in}-\frac{\pi}{4}\right)+1\}$$

$$= 16\ \alpha^2 {A_{in}}^2. \qquad (11)$$

The equation (11) shows the overall rectified DC output is independent to the input progressive phase shift ϕ_{in}, showing the full-FoV WPT capability. Based on the equation (3), (5), (7), and (9), the 4 incoming RF signals are phase shifted and not simply combined. Thus, with the passive beamforming technique, the proposed beam-former can support concurrent multi-direction/-beam signal process. Compared to the conventional 1×4 rectenna array (overall rectified DC output is $4A^2\beta$), the equation (11) shows an array factor (4×) improvement, which is proportional to its array size and can be scalable to a large scaled N-element array with a N×N Butler matrix. Although the passive loss coefficient α^2 degrades overall performance, the compact low-loss passive beam-former is designed to accommodate this issue and the detailed analysis will be shown in the chapter II-C.

The equations (3)~(11) are further verified by the ADS simulations. An ideal 4×4 Butler matrix with coupled line-based schematic is shown in Fig. 9. The four inputs are injected by voltage source ports with programmable phase shifts to synthesize the array field-of-view operation. The S-parameter simulation (Fig. 10) shows that the RF signal is well beam-formed as ϕin = +45˚, -45˚, +135˚, -135˚ where the incidence shows that one of the 4 outputs is with array factor as well as a peak value and the rest three outputs are near to zero RF power. However, it doesn't mean that the other incident angle would not preserve the array factor enhancement since the other three outputs are then started to generate RF outputs to the following rectifiers. For instance, when the ϕin = 0˚, +90˚, -90˚, +180˚, -

180˚, selected two of 4 outputs generate slightly lower RF power (3dB lower compared to the peak value) and the rest two outputs still provide lower yet decent power. Thus, by summing the mentioned RF power after the rectification, the overall DC power is possibly be large. To verify this observation and equation (11), the 4 outputs are then simulated with an ideal 1×4 rectifier arrays and the DC power combiner shows that the normalized power is flat over full field-of-view, agreeing well with the theoretical derivation (Fig. 11).

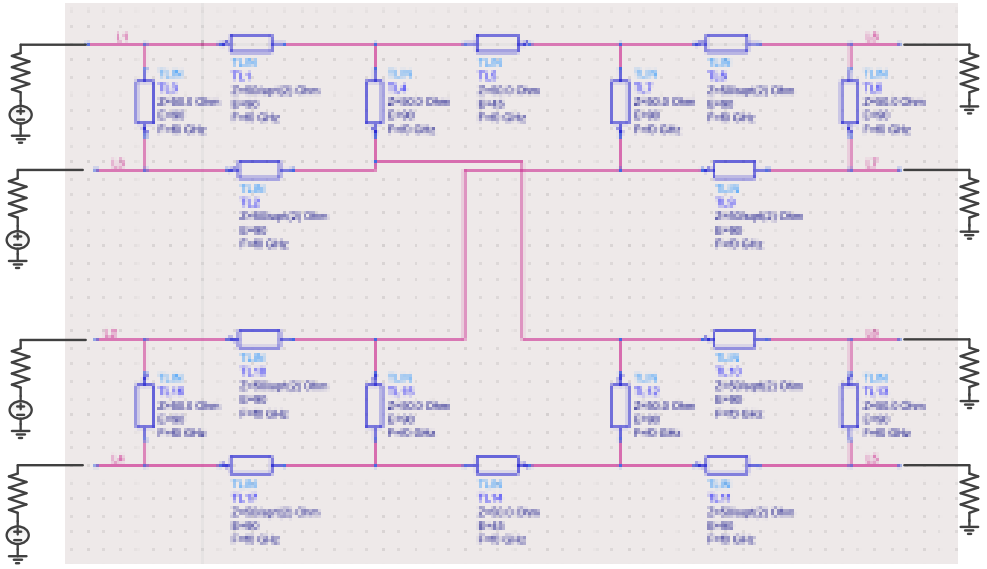

Figure 9. Ideal coupled-line based 4×4 Butler matrix schematic of the proposed rectenna array

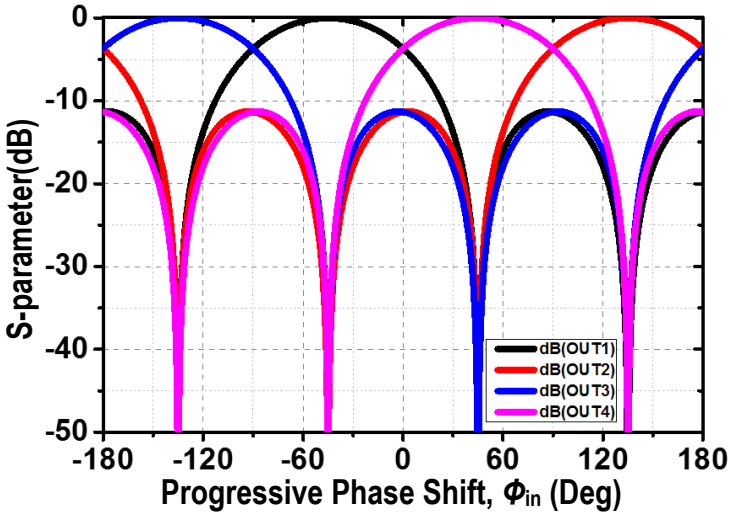

Figure 10. Simulated S-parameter for the ideal Butler matrix schematic of the proposed rectenna array

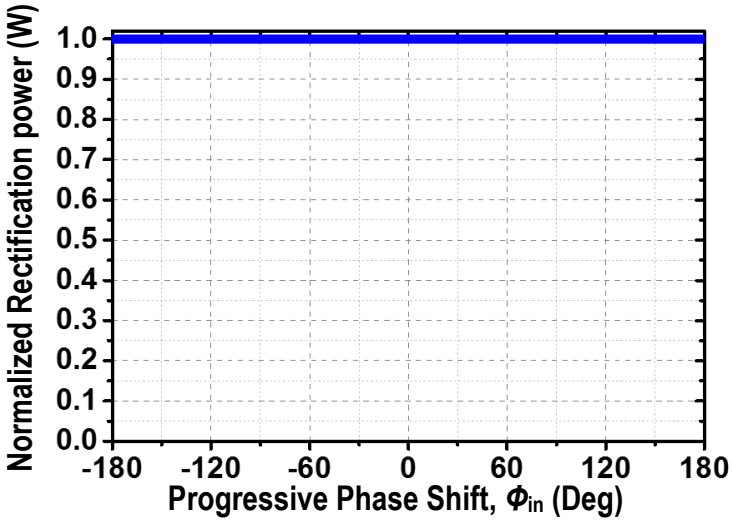

Figure 11. Simulated receiving DC power of the proposed 1×4 rectenna array

C. Ultra-compact 4×4 Butler matrix design

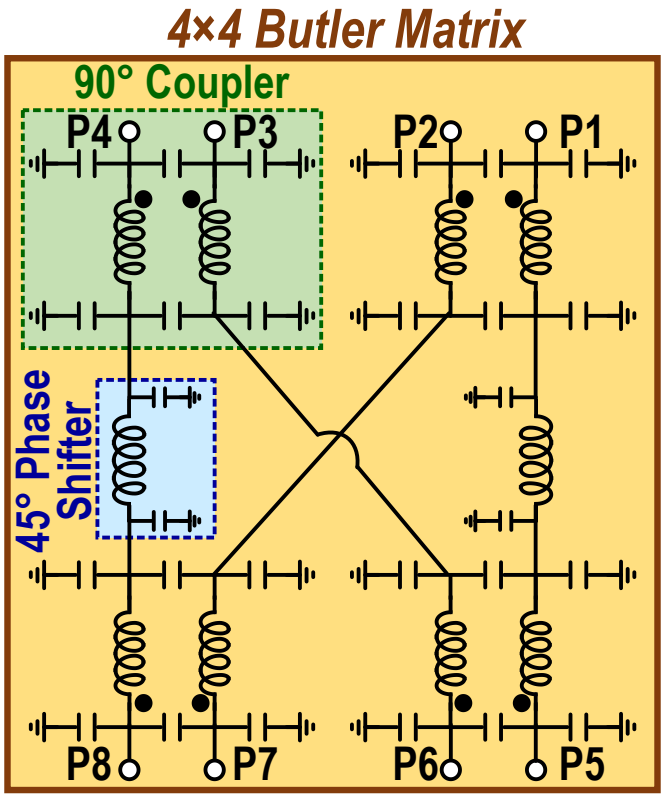

Figure 12. Schematic of the proposed 4×4 Butler matrix

To achieve 100× size reduction compared to conventional Butler matrix design [19], transformer-based 90˚ coupler and compact lumped-element LC based 45˚ phase shifter are implemented [20]-[22] in the proposed 4×4 Butler matrix design (Fig. 12). First, the compact transformer 90 coupler is analyzed in detail. The schematic of the transformer-based quadrature hybrid [20] is shown in Fig. 13(a). The circuit analysis on this hybrid structure presents a relationship between coupling coefficient and size reduction. Compact high-coupling transformer quadrature hybrid is then proposed in the passive beamformer.

When driven signal only at the input port (IN), both inductive and capacitive couplings are used in this transformer-based network to achieve matched quadrature output signals at the through port (THRU, -90°) and the coupled port (CPL, 0°), shown in Fig. 13(a). The inductive coupling coefficient k_L and the capacitive coupling coefficient k_C are defined in equations (12) and (13), respectively. L_M and C_M indicate the mutual inductance and mutual capacitance, and the quantity C is defined as C_M+C_G.

$$k_L = \frac{L_M}{L} \tag{12}$$

$$k_C = \frac{C_M}{\sqrt{(C_G + C_M)(C_G + C_M)}} = \frac{C_M}{C} \tag{13}$$

Next, the design is analyzed by even-/odd-mode analysis. For the even-mode operation ($V_{ex1}=V_{ex2}=V_0$), a virtual open-circuit condition exists along the symmetric line in Fig. 13(a), and a positive magnetic coupling ($i_1=i_2$) is achieved. Then, the equivalent even-mode half-circuit can be formed as a C-L-C pi-network with the even-mode inductance $L_e=L(1+k_L)$ and the even-mode capacitance $C_e=C(1-k_C)$, shown in Fig. 13(b). The even-mode characteristic impedance Z_{0e} and propagation velocity v_e are given in (14) and (15), and the even-mode voltages at all the nodes (V_{1e}-V_{4e}) are shown in (16) and (17). Note that V_{3e} and V_{4e} are the input and output voltages for the other and identical even-mode half circuit, which is not shown in Fig. 13(b).

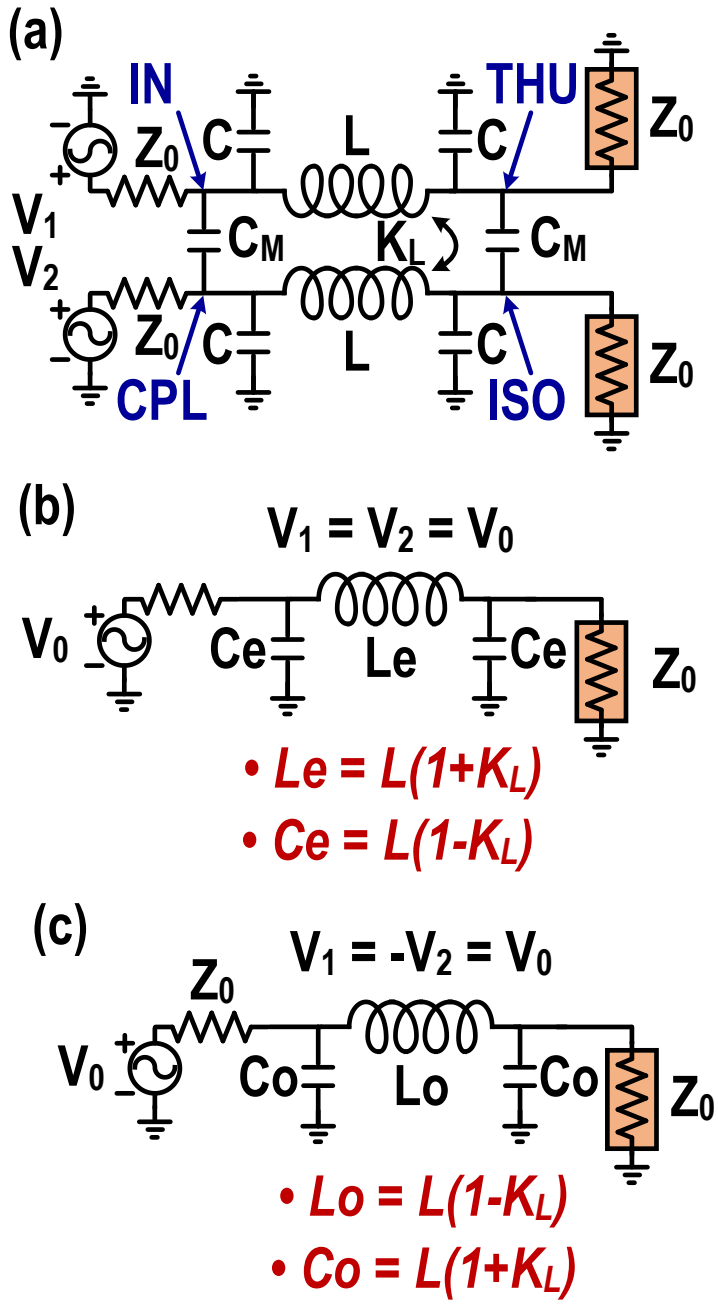

Figure 13. The (a) transformer-based quadrature hybrid schematic and (b) its even-mode half-circuit and (c) odd-mode half-circuit.

$$Z_{0e} = \sqrt{\frac{L_e}{C_e}} = \sqrt{\frac{L(1+k_L)}{C(1-k_C)}} \tag{14}$$

$$v_e = \frac{1}{\sqrt{L_e C_e}} = \frac{1}{\sqrt{L(1+k_L)C(1-k_C)}} \tag{15}$$

$$V_{1e} = V_{3e} = V_0 \frac{(\frac{1}{SC_e} // Z_0 + SL_e) // \frac{1}{SC_e}}{Z_0 + (\frac{1}{SC_e} // Z_0 + SL_e) // \frac{1}{SC_e}} \tag{16}$$

$$V_{2e} = V_{4e} = V_{1e} \frac{\frac{1}{SC_e} // Z_0}{\frac{1}{SC_e} // Z_0 + SL_e} \tag{17}$$

On the other hand, the odd-mode operation is then analyzed, i.e., V_{ex1}=-V_{ex2}=V_0, a virtual ground is created along the symmetric line in Fig. 13(a), and the magnetic coupling (i_1=-i_2) is negative. Therefore, the odd-mode inductance L_o equals L(1-k_L), and the odd-mode capacitance C_o equals C(1+k_C), shown in the odd-mode half-circuit in Fig. 1(c). The odd-mode characteristic impedance Z_{0o}, propagation velocity v_o, and the voltages at all the nodes (V_{1o}-V_{4o}) are shown in equations (18)-(21). Note that V_{3o} and V_{4o} are the input and output voltages for the other and identical odd-mode half circuit, which is not shown in Fig. 1(c).

$$Z_{0o} = \sqrt{\frac{L_o}{C_o}} = \sqrt{\frac{L(1-k_L)}{C(1+k_C)}} \tag{18}$$

$$v_o = \frac{1}{\sqrt{L_o C_o}} = \frac{1}{\sqrt{L(1-k_L)C(1+k_C)}} \tag{19}$$

$$V_{1o} = -V_{3o} = V_0 \frac{(\frac{1}{SC_o} // Z_0 + SL_o) // \frac{1}{SC_o}}{Z_0 + (\frac{1}{SC_o} // Z_0 + SL_o) // \frac{1}{SC_o}} \tag{20}$$

$$V_{2o} = -V_{4o} = V_{1o} \frac{\frac{1}{SC_o} // Z_0}{\frac{1}{SC_o} // Z_0 + SL_o} \tag{21}$$

To further capture the intrinsic parameter of the equations, the transformer-based quadrature hybrid can be treated as a one-section synthetic coupled transmission line and

apply the ABCD/S-parameter matrix to solve it. The 4-port S-parameters of the transformer-based quadrature hybrid can be obtained by the equations (22)-(26).

$$S_{11} = S_{22} = S_{33} = S_{44} = \frac{Z_{in} - Z_0}{Z_{in} + Z_0} \tag{22}$$

$$Z_{in} = Z_0 \frac{(V_{1e} + V_{1o})}{(2V_0 - V_{1e} - V_{1o})} \tag{23}$$

$$S_{21} = S_{12} = (V_{2e} + V_{2o})/V_0 \tag{24}$$

$$S_{31} = S_{13} = V_{3e} + V_{3o} = (V_{1e} - V_{1o})/\, V_0 \tag{25}$$

$$S_{41} = S_{14} = (V_{4e} + V_{4o})/V_0 \tag{26}$$

To achieve quadrature signal generation 90˚ phase difference, the equivalent coupled transmission line should behave as a quarter-wave line at the frequency $\omega_{\lambda/4}$. assume that the IN-port is excited by a source voltage of $2V_{IN}(\omega_{\lambda/4})$, the CPL-port and THRU-port outputs at the operation frequency are given as

$$\frac{V_{CPL}(\omega_{\lambda/4})}{V_{IN}(\omega_{\lambda/4})} = \frac{Z_{0e} - Z_{0o}}{Z_{0e} + Z_{0o}} = k \tag{27}$$

$$\frac{V_{THRU}(\omega_{\lambda/4})}{V_{IN}\,(\omega_{\lambda/4})} = -j\sqrt{1 - k^2}. \tag{28}$$

Therefore, the excitation at the IN-port will result in quadrature signals at the CPL-port and THRU-port. The complete design parameters for a transformer-based quadrature generation network can be uniquely specified by the equations (29)-(31) at the frequency $\omega_{\lambda/4}$.

$$\frac{C_M}{C} = k \tag{29}$$

$$Z_0 = \sqrt{Z_{0e}Z_{0o}} = \sqrt{\frac{L}{C}} \tag{30}$$

$$\omega_{\lambda/4} = \frac{1}{\sqrt{LC(1 - k^2)}} \tag{31}$$

Based on (27)-(31), it clearly shows that the coupling coefficient k is an essential design parameter for the transformer-based quadrature hybrid, since it determines the output magnitudes of the CPL-port and the THRU-port as well as the required inductance and capacitance at the operation frequency $\omega_{\lambda/4}$.

Based on the designed coupling coefficient K and operation frequency, the proof-of-concept compact transformer-based 90˚ coupler is created. A similar methodology is also applied into a passive 45° synthetic transmission line by using LC lumped circuit. A proof-of-concept compact 4×4 Butler matrix is then designed at 2.4GHz as the compact passive beamformer for the proposed WPT. The design is fabricated with a hybrid FR4-Rogers PCB board Fig.14 The 3D EM HFSS structure and the PCB design are shown in Fig. 5a. It occupies a compact 42mm×50mm, achieving 100× size reduction than conventional coupled-line based Butler matrix design [19].

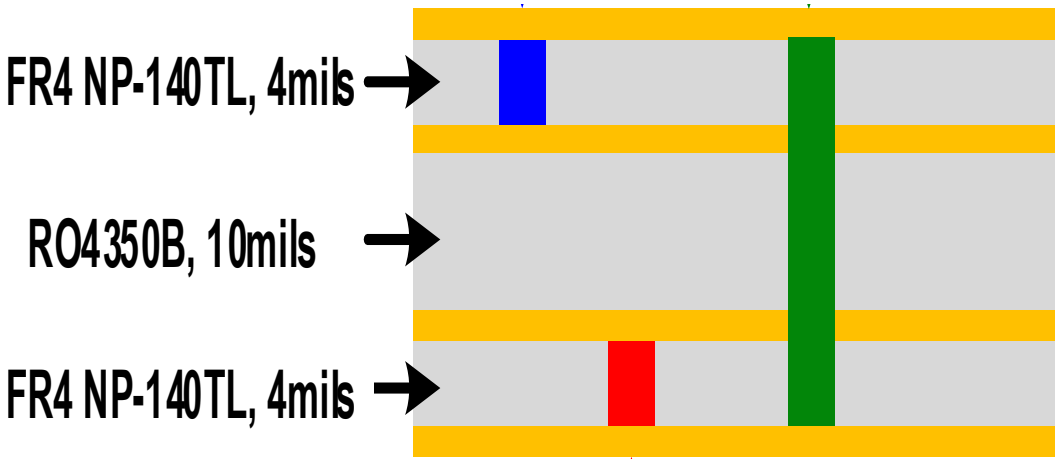

Figure 14. 4-layer FR4-Rogers hybrid PCB stack-up

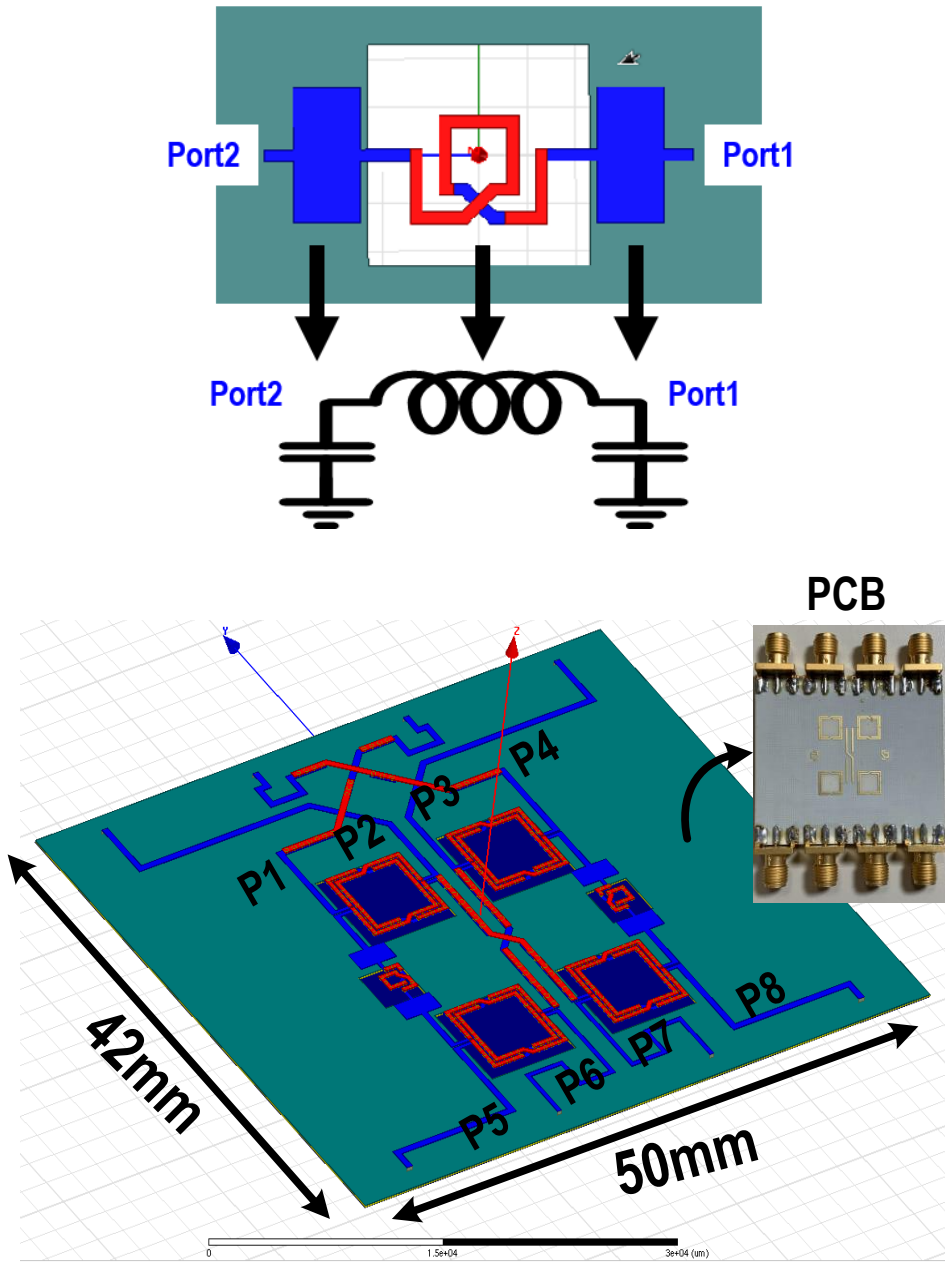

Figure 15. 3D EM HFSS of the 45˚ phase shifter and the proposed 4×4 Butler matrix as well as the PCB design

The overall measurements including the parasitic effects from the SMA connectors are plotted in Fig. 16. At 2.4GHz, it achieves input matching <-17dB, insertion loss <0.8 dB, amplitude mismatch <0.3dB, and peak-to-null ratio >35dB, outperforming the state-of-the-art designs.

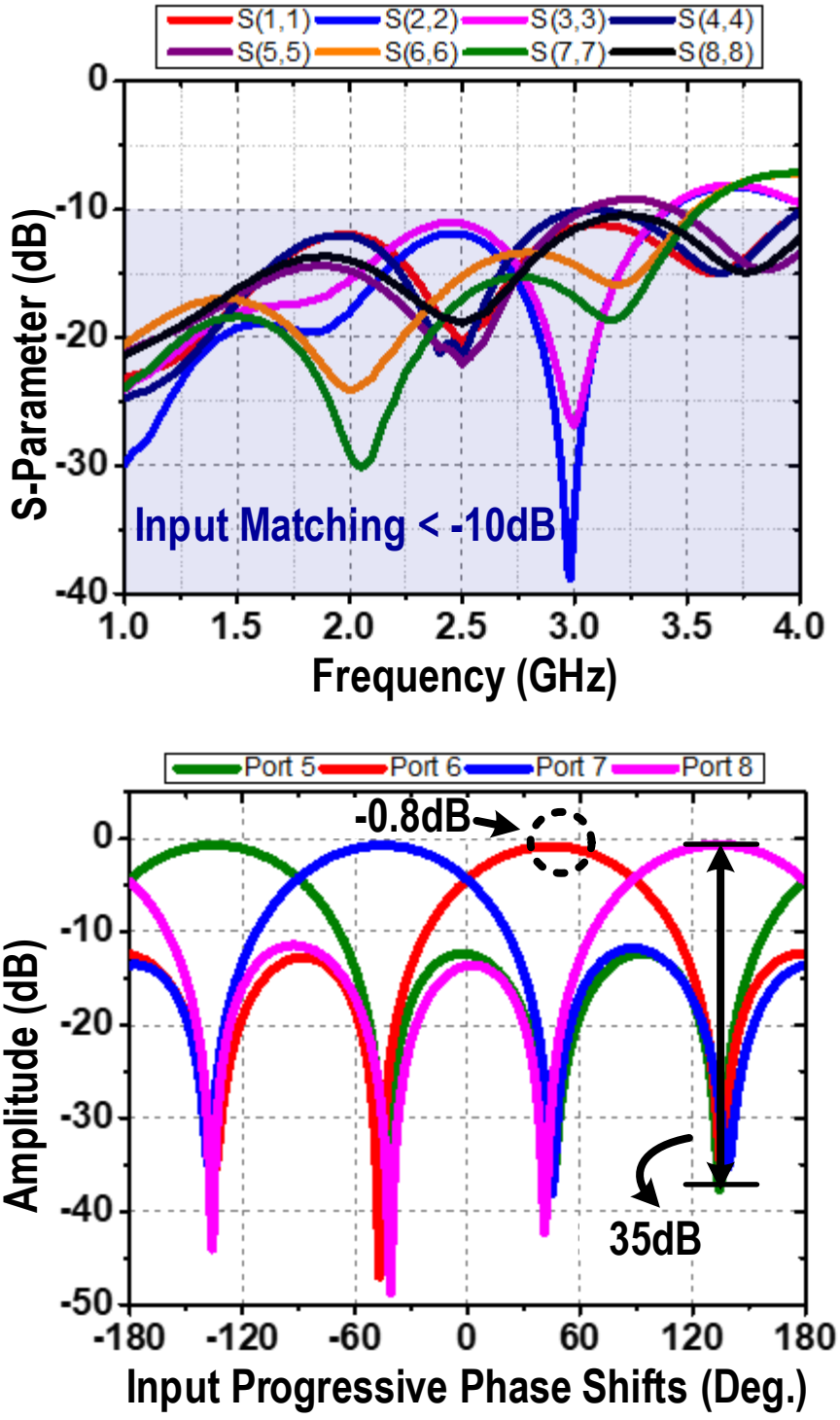

Figure 16. Measured amplitude performance of the proposed 4×4 Butler matrix

D. High-efficiency rectifier design

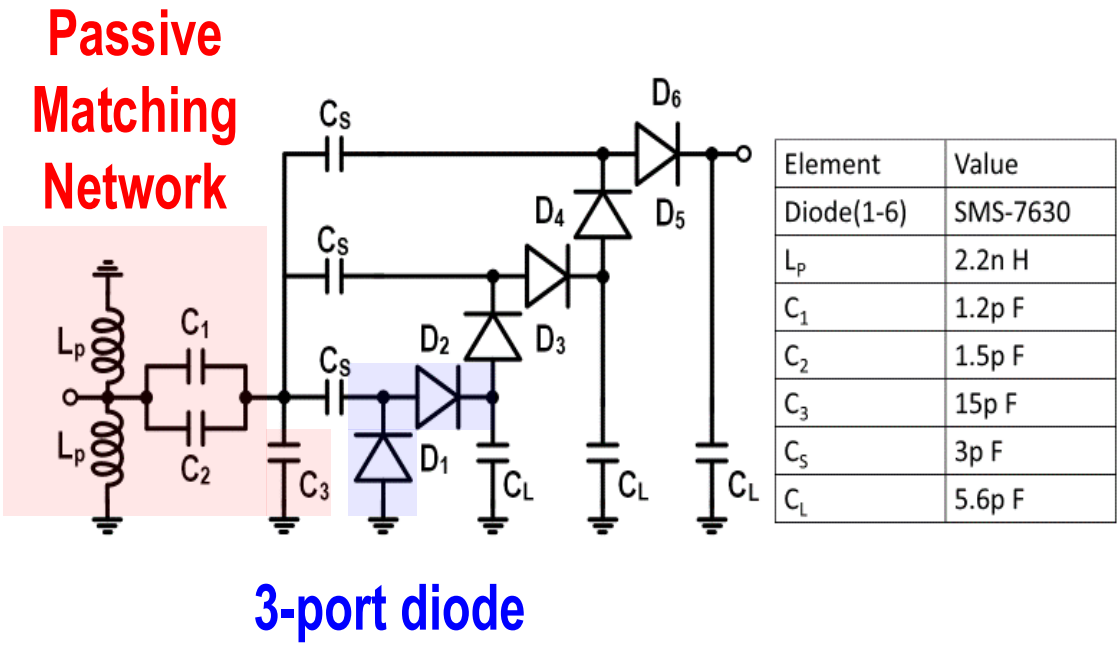

Element	Value
Diode(1-6)	SMS-7630
L_P	2.2n H
C_1	1.2p F
C_2	1.5p F
C_3	15p F
C_S	3p F
C_L	5.6p F

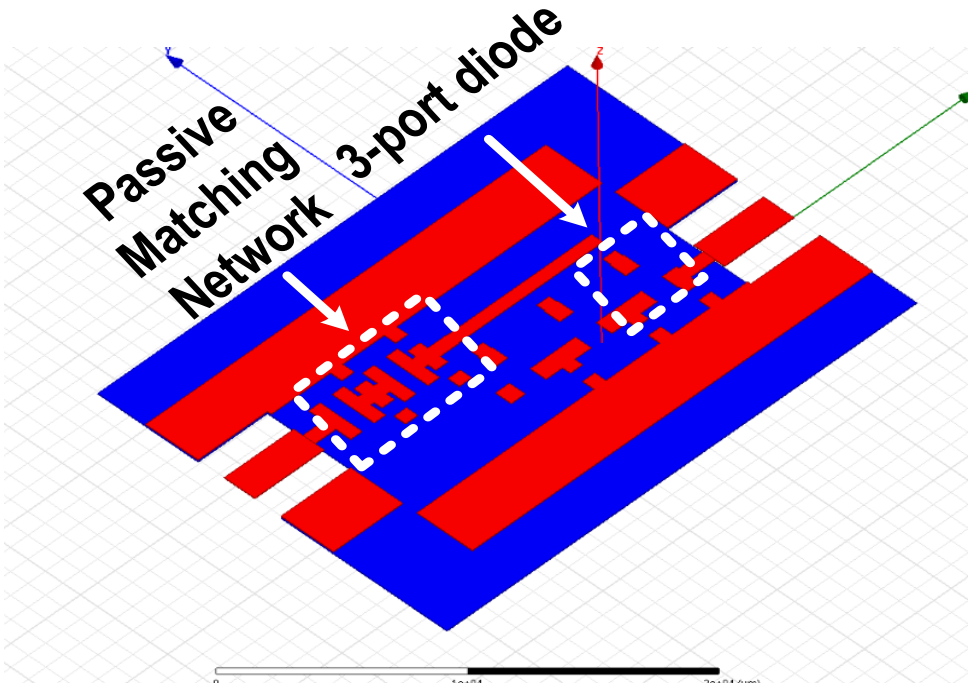

Figure 17. A 3-stage Dickson voltage doubler design example and its 3D EM HFSS model

To optimize the output rectification stage, there are two types of rectifier design studied, analyzed, and discussed in the thesis. First, the RF-to-DC Dickson voltage doubler

is normally used to enhance output DC voltage swing. A 3-stage Dickson voltage doubler design example is shown in the Fig. 17. Input matching network is used to transform 50ohm of the Butler matrix to high impedance node of the doubler. Passive voltage amplification is applied to improve the operation for the rectification stage with better efficiency. CL for each stage is used to double the voltage and serves as DC charge capacitors. On the other hand, the Cs is used for controlling the switching time for the response the rectification stage. The voltage doubler is typically used to improve the conversion between RF power and DC voltage rather than RF power to DC power. To further enhance rectification efficiency, the conversion for RF power to DC power can be explored in a single stage high-efficiency design in the Fig. 18. The high-efficiency rectifier design is only using one diode to avoid parasitic capacitors to ground and a radial stub is used to extend its operation frequency. Less parasitic capacitors to ground and multi-session series inductor is used to peak up the voltage gain, demonstrating its higher RF-to-DC power conversion. Moreover, it normally requires less loaded Q transformation and thus can use a simple one section inductor to facilitate input match rather than shunt capacitor to ground to decrease the loaded Q. Easier matching scheme is achieved compared to the Dickson voltage doubler and it will be combined with the Butler matrix as final proposed WPT network.

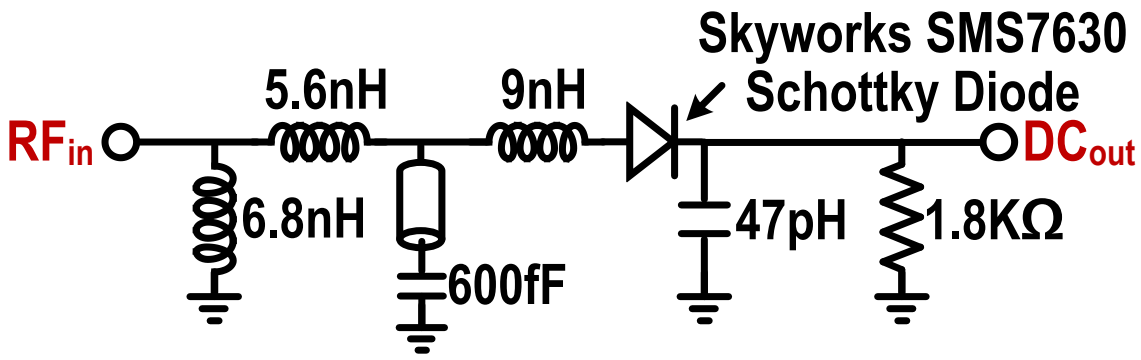

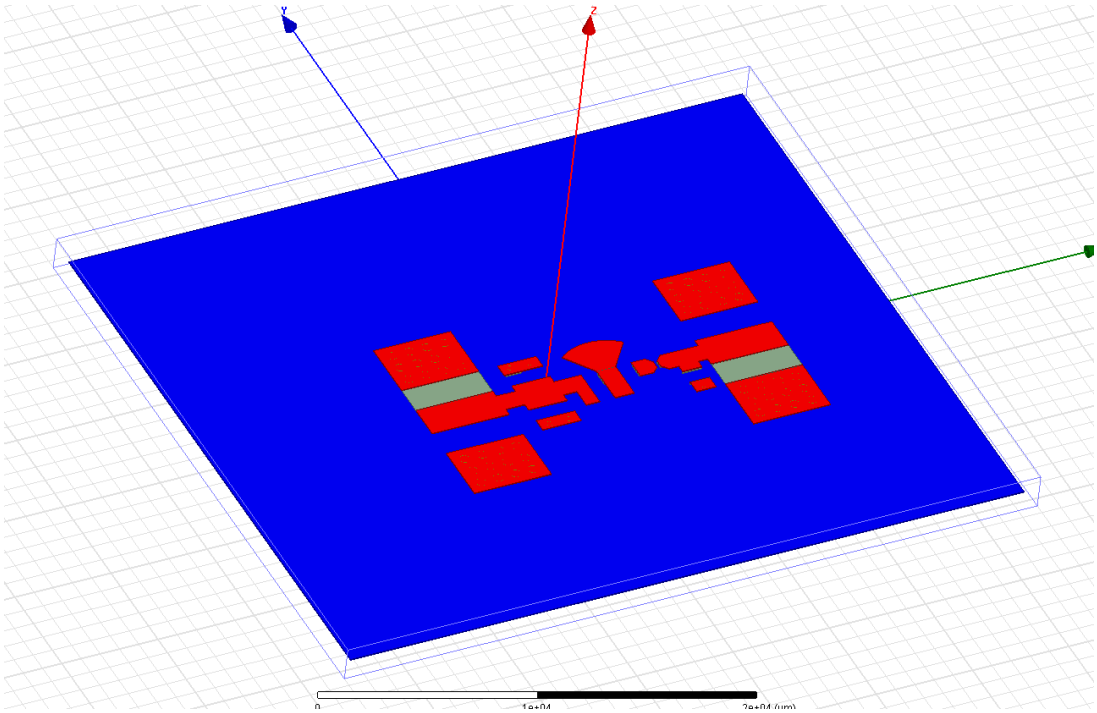

Figure 18. A high-efficiency rectifier design example and its 3D EM HFSS model

E. Wideband end-fire bow-tie antenna design

To receive full field-of-view RF signals, the end-fire bow-tie antenna design is applied to cover input progressive phase shift from -180˚ to 180˚ (Fig. 19). Inputs of the antenna are fed by a single-to-differential bending transmission line. The ground (green color) is used to end-fire beam to the front side and isolate the substrate mode effect to the antenna. Moreover, the wideband design is also considered during the extended ground plane, which can serve dual LC resonance for the antenna. Returning current in ground plane is also further explored to ensure the radiation efficiency is higher than 80%. The antenna is then fabricated in 2-layer rogers board RO3006 with 50 mil thickness and the prototype is also shown in Fig. 19 with its 3D EM HFSS model, occupying a size 250mm × 82mm at 2.4GHz. The prototype antenna array will be demonstrated with the 1×4 proposed high-efficiency rectenna array for WPT. The detailed measurement for the far-field WPT will be shown in the Chapter 3.

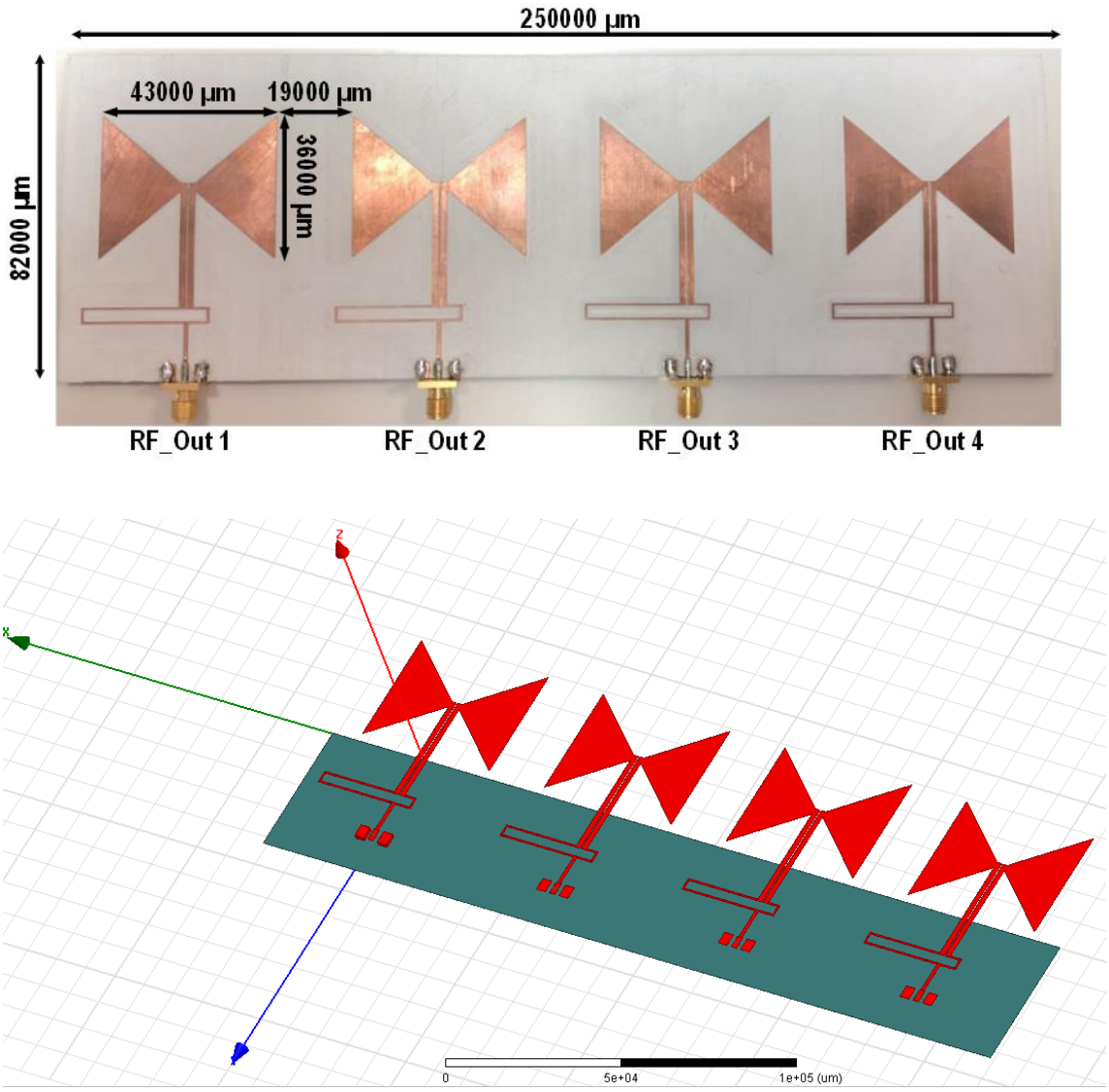

Figure 19. A 1×4 bow-tie end-fire antenna array design example and its 3D EM HFSS model

CHAPTER III

MEASUREMENTS RESULTS

First, the single-stage rectifier is measured to test rectification efficiency versus different input RF power. The fabricated 4-layer PCB (Fig. 14) for WPT is shown on the Fig. 20. It includes a Skyworks SMS7630 Schottky diode, L1 (6.8nH), L2 (5.6nH), L3 (4.7nH), and L4 (4.3nH) for input matching as well as the output C1 (47pH) and optimal load 1.8Kohm. Keysight signal source E8257D and oscilloscope MSO9404A are used to characterize the RF-to-DC conversion.

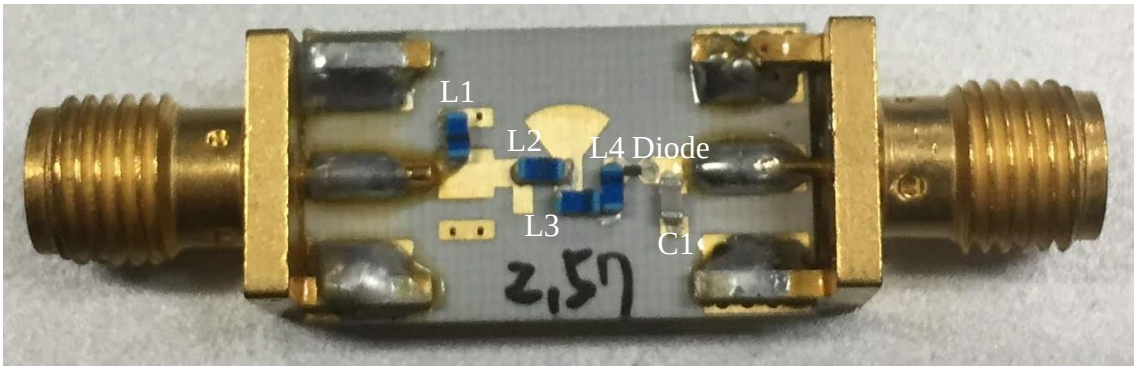

Figure 20. A fabricated high-efficiency rectifier sample

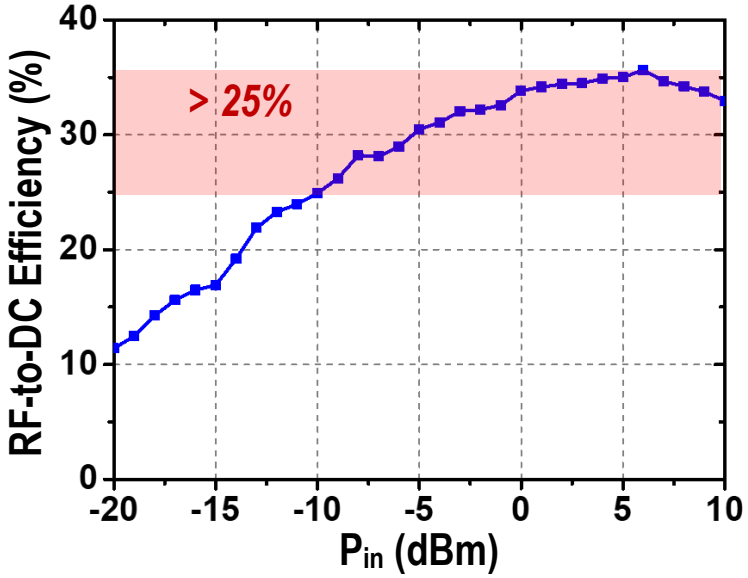

Figure 21. Measured RF-to-DC efficiency versus the RF Pin

In Fig. 21, with the input matching network loss, it shows high sensitivity with >25% efficiency at a Pin of -10dBm and with a peak 35.5% efficiency at moderate RF input power Pin = 6dBm. Four of the fabricated rectifier designs are then combined into the proposed WPT network.

The proposed concurrent multi-direction array-based high-efficiency is also fabricated with the 4-layer PCB (Fig. 14). It consists of a 4×4 Butler matrix and a 1×4 rectifier array with a compact overall size 50mm×65mm, shown in Fig. 22.

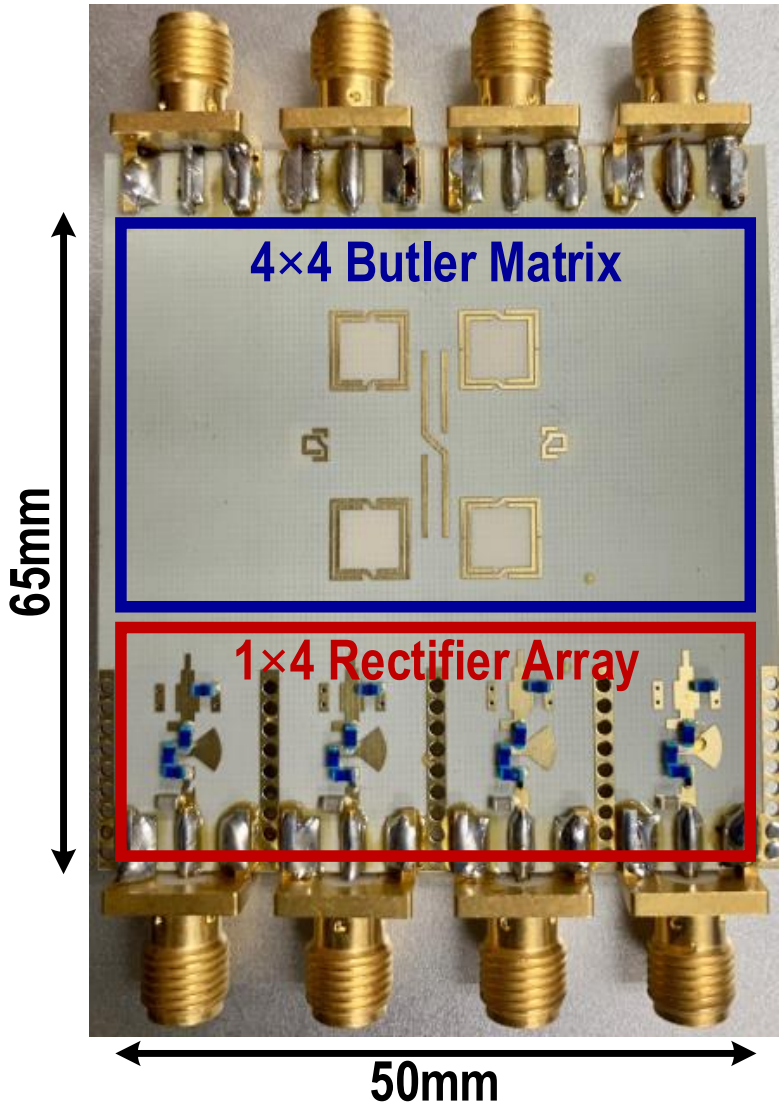

Figure 22. A fabricated concurrent multi-direction array-based high-efficiency WPT sample

The proposed WPT network is then characterized by the 4-channel AWG 8195A and the conventional simple 1×4 rectenna array is also tested for comparison. AWG 8195A in the measurement setup (Fig. 23) is utilized to generate programmable phase shift to synthesize the phased array FoV operation and the oscilloscope MSO9404A is used to characterize the RF-to-DC conversion. The proposed WPT circuit and conventional rectenna array are then tested and compared in the Fig. 24.

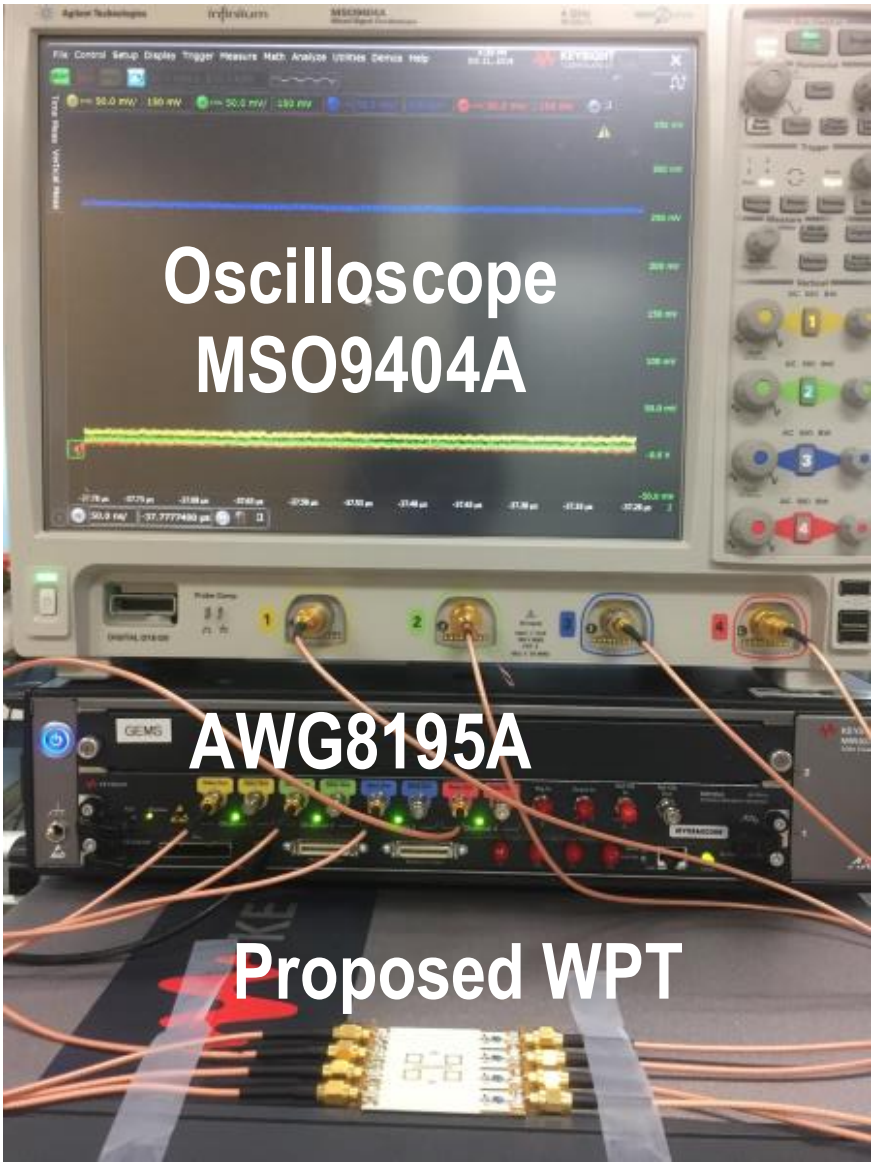

Figure 23. Measurement setup for the synthesized phased array generation and the rectenna array characterization

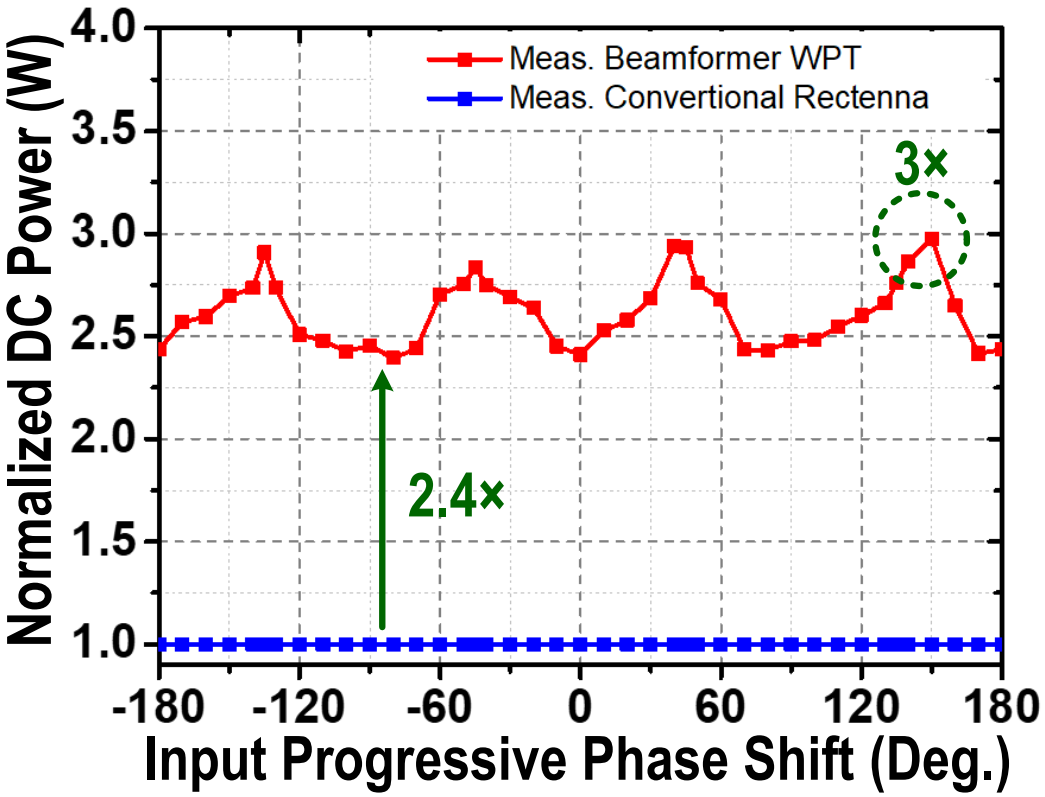

Figure 24. Measured normalized DC power for proposed WPT and conventional design

In Fig. 24, it can clearly be seen that both the conventional 1×4 rectenna array design and the proposed 1×4 WPT design preserve full-FoV WPT operation. However, the proposed design has at least a 2.4× enhancement and with a peak 3× improvement on received power and efficiency over the conventional design (ideal case is with at least 4× improvement without any passive loss).

To facilitate the proposed WPT operation in the future wireless sensor IoT application, far-field wireless measurement is also demonstrated. Antenna array is firstly captured for its input matching (Fig. 19 and Fig. 25). The dual resonance design mentioned in chapter II-E is observed in the measurement, showing S11<-10dB across 2.2G - 3.1GHz wideband operation. Then, the figure 26 shows a far-field measurement setup for the proposed WPT. The antenna arm is also swept for the measurement under different E-/H-plane and field-of-view receiving characterization.

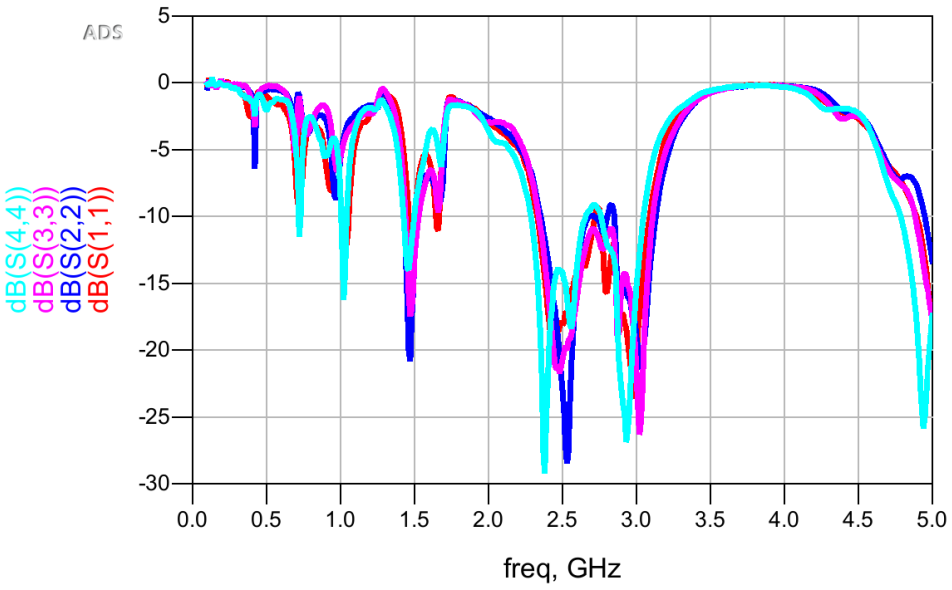

Figure 25. Measured input matching for each input of the 1×4 antenna array

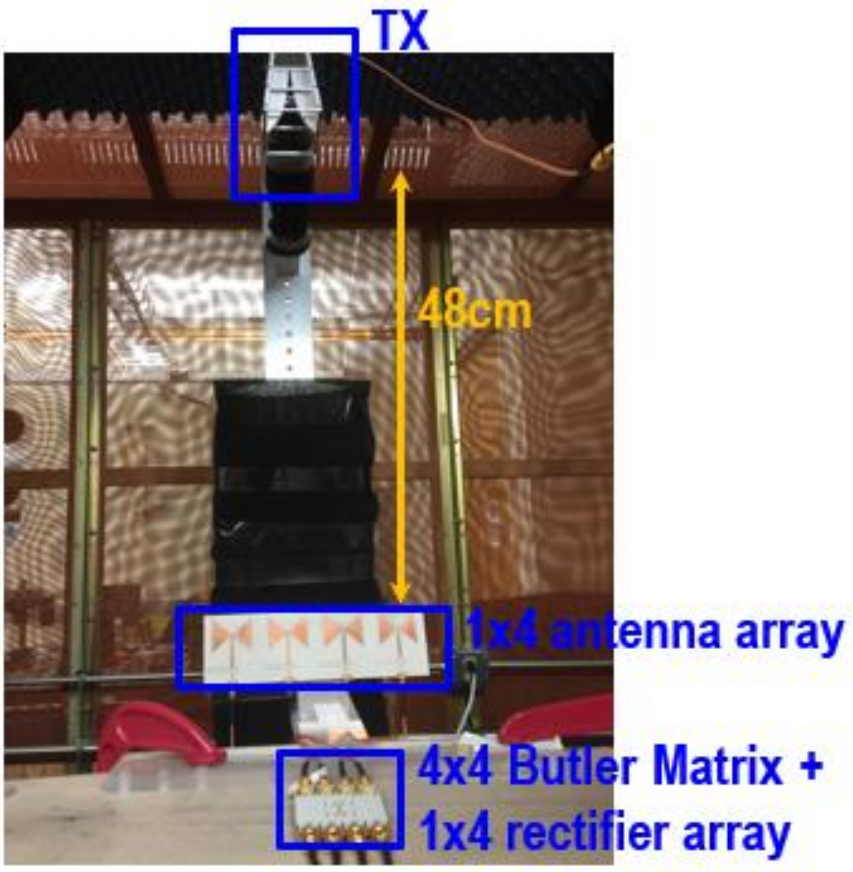

Figure 26. Far-field measurement setup

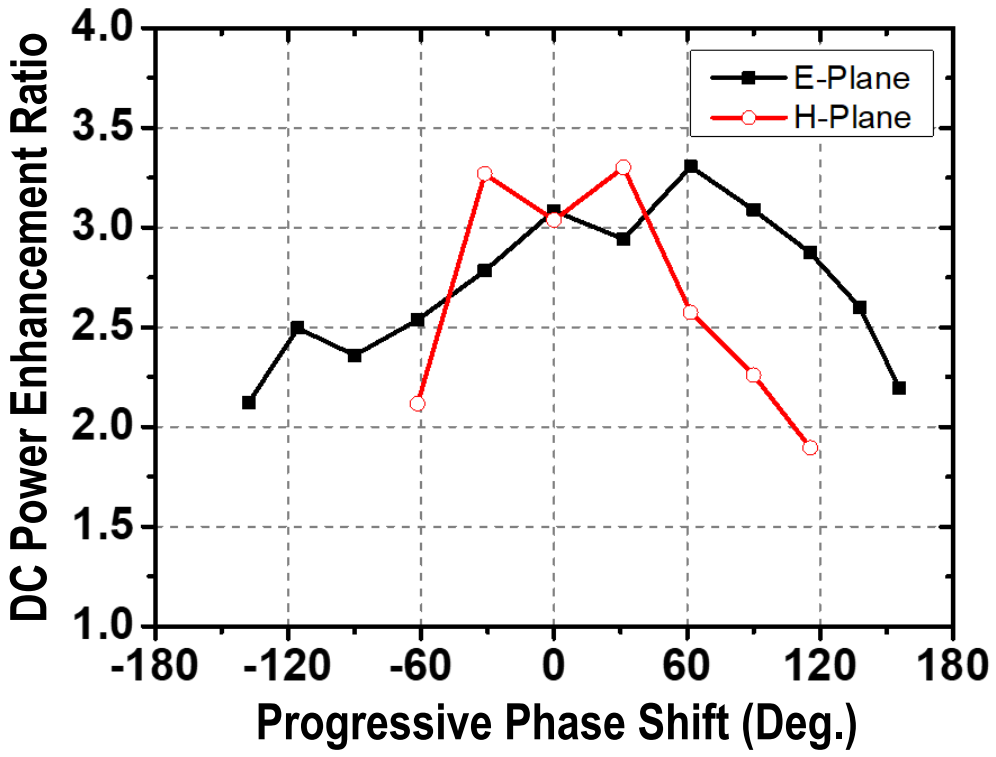

Figure 27. Measured normalized DC power for proposed WPT and conventional design in far-field

The proposed WPT design is also compared with conventional 1×4 rectenna array design in the far-field measurement shown in Fig. 27. It shows a peak 3× improvement than the conventional design and covers a wide field-of-view operation. Moreover, compared to AWG ideal array generation, the DC power enhancement in the far-field measurement degrades substantially when the receiving RF signals are injected near end-fire region. This is because there is none of an antenna can support flat gain at end-fire angle, i.e. -180˚ and +180˚, even with the end-fire antenna design. However, the proposed design still can leverage its antenna design limitation with at least 2× over -150˚ and +150˚ (overall 300˚ field-of-view operation) then conventional 1×4 rectenna design.

CHAPTER VI

CONCLUSION

In this thesis, an ultra-compact concurrent multi-directional beamforming receiving network for high-efficiency WPT is proposed and demonstrated. It achieves high-quality passive beam-former based rectenna array with low-loss, compact size, and high RF-to-DC conversion efficiency. We first present a theorical analysis for three different types of the rectenna array including (1) conventional rectenna array with simple DC power summing, (2) passive simple power combiner based rectenna array, and (3) our proposed array-based beamforming high-efficiency rectenna array design. Clear descriptions are addressed and proved by the theoretical derivation, showing that our proposed circuit exhibits array factor enhancement over full field-of-view to significantly improve the received DC power compared to the state-of-the-art designs. Moreover, the scalability of the proposed design is also proved in the derivation. With N-element phased array, it can improve at least N× RF-to-DC power conversion. Next, a compact transformer-based Butler matrix is also analyzed with the capacitive and magnetic coupling factors. Even- and odd-mode analysis are applied to the design for facilitating the compact quadrature hybrid and 45˚ phase shifter. For far-field WPT, an end-fire bow-tie antenna array is explored in the design to extend the wide field-of-view operation.

Then, the proposed high-efficiency WPT array is fabricated in the hybrid FR4-Rogers PCB board. It is first tested with the AWG M8195A and shows at least 2.4× efficiency enhancement compared to the conventional design and cover full field-of-view with no degradation. Far-field wireless measurement also demonstrates the proposed WPT can process at least 2× RF-to-DC conversion than conventional design under the wide field-of-view (300˚). In conclusion, this is the first demonstration for ultra-compact concurrent multi-directional beamforming receiving network for high-efficiency WPT with clear analysis and complete measurements, outperforming the state-of-the-arts (Table 1).

TABLE I
COMPARISON OF STATE-OF-THE-ART RECTENNA ARRAYS

	Rectenna Array	Frequency (GHz)	2D concurrent beamforming	Array factor enhancement	Topology	Field-of-view (degree)
Z. Popovic TMTT 14'	Yes	2.45	No	No	Antenna arrays + rectifier arrays	50
A. Takacs IMS 14'	No	14.5	No	No	Antenna + rectifier	N/A
Nina P. Basta WPTC 15'	Yes	2.3	No	No	2D complementary Antenna arrays + rectifier arrays	N/A
A. Takacs IMS 15'	No	14.7	No	No	Antenna + rectifier	N/A
This work	**Yes**	**2.4**	**Yes**	**Yes**	**Full field-of-view Antenna beamforming network + rectifier arrays**	**360**

REFERENCES

[1] G. A. Covic and J. T. Boys, “Inductive power transfer,” Proc. IEEE, vol. 101, no. 6, pp. 1276–1289, Jun. 2013.

[2] W. Brown, “The history of power transmission by radio waves,” IEEE Trans. Microw. Theory Techn., vol. MTT-32, no. 9, pp. 1230–1242, Sep. 1984.

[3] N. Shinohara and H. Matsumoto, “Experimental study of large rectenna array for microwave energy transmission,” IEEE Trans. Microw. Theory Techn., vol. 46, no. 3, pp. 261–268, Mar. 1998.

[4] L. Epp, A. Khan, H. Smith, and R. Smith, “A compact dual-polarized 8.51-GHz rectenna for high-voltage (50 V) actuator applications,” IEEE Trans. Microw. Theory Techn., vol. 48, no. 1, pp. 111–120, Jan. 2000.

[5] B. Strassner and K. Chang, “Microwave power transmission: Historical milestones and system components,” Proc. IEEE, vol. 101, no. 6, pp. 1379–1396, Jun. 2013.

[6] J. A. Hagerty, F. Helmbrecht, W. McCalpin, R. Zane, and Z. Popović, “Recycling ambient microwave energy with broadband antenna arrays,” IEEE Trans. Microw. Theory Techn., vol. 52, no. 3, pp. 1014–1024, Mar. 2004.

[7] E. Falkenstein, M. Roberg, and Z. Popović, “Low-power wireless power delivery,” IEEE Trans. Microw. Theory Techn., vol. 60, no. 7, pp. 2277–2286, Jul. 2012.

[8] G. Vera, A. Georgiadis, A. Collado, and S. Via, “Design of a 2.45 GHz rectenna for electromagnetic (EM) energy scavenging,” in IEEE Radio Wireless Symp., 2010, pp. 61–64.

[9] Z. Popović, E. Falkenstein, D. Constinett, and R. Zane, “Low-power far-field wireless powering for wireless sensors,” Proc. IEEE (Special Issue), vol. 101, no. 6, pp. 1397–1409, Jun. 2013.

[10] Z. Popovic et al., “Scalable RF energy harvesting,” IEEE Trans. Microw. Theory Techn., vol. 62, no. 4, pp. 1046–1056, Apr. 2014.

[11] A. Takacs et al., “Compact Rectenna for Space Application,” Proc. IEEE International Microwave Symposium (IMS), May 2014

[12] Nina P. Basta et al., “Bow-Tie Rectenna Arrays,” IEEE WPTC 2015 Digest. pp 1-4

[13] A. Takacs et al., “Ultra-Compact Ku band Rectenna” Proc. IEEE International Microwave Symposium (IMS), May 2015

[14] D. Lee et al., “Hybrid Power Combining Rectenna Array for Wide Incident Angle Coverage in RF Energy Transfer,” IEEE Trans. Microw. Theory Techn., Mar. 2017.

[15] M. Huang, T. Chi, and H. Wang, "A 5GHz All-Passive Negative Feedback Network for RF Front-End Self-Steering Beam-Forming with Zero DC Power Consumption,” Proc. IEEE Radio Frequency Integrated Circuits (RFIC), May 2016.

[16] M. Huang, T. Chi, F. Wang, and H. Wang, “An All-Passive Negative Feedback Network for Broadband and Wide Field-of-View Self-Steering Beam-Forming with Zero DC Power Consumption,” IEEE J. of Solid-State Circuits, vol. 52, no. 5, pp. 1260 - 1273, May 2017.

[17] M. Huang, T. Chi, F. Wang, T. Li, and H. Wang, "A 23-to-30GHz Hybrid Beamforming MIMO Receiver Array with Closed-Loop Multistage Front-End Beamformers for Full-FoV Dynamic and Autonomous Unknown Signal Tracking and Blocker Rejection," IEEE International Solid-State Circuits Conference (ISSCC) Dig. Tech. Papers, Feb. 2018.

[18] M. Huang and H. Wang, "A 27-41GHz MIMO Receiver with N-Input-N-Output Using Scalable Cascadable Autonomous Array-Based High-Order Spatial Filters for Instinctual Full-FoV Multi-Blocker/Signal Management," IEEE International Solid-State Circuits Conference (ISSCC) Dig. Tech. Papers, Feb. 2019.

[19] K. Wincza, S. Gruszczynski, and K. Sachse, “Broadband planar fully integrated 8 8 Butler matrix using coupled-line directional couplers,” IEEE Trans. Microw. Theory Techn., vol. 59, no. 10, pp. 2441–2446, Oct. 2011.

[20] J. Park and H. Wang, “A Transformer-Based Poly-Phase Network for Ultra-Broadband Quadrature Signal Generation,” IEEE Trans. Microw. Theory. Tech, vol. 63, no. 12, pp. 4444 - 4457, Dec. 2015.

[21] E. Garay, M. Huang, and H. Wang, "A Cascaded Self-Similar Rat-Race Hybrid Coupler Architecture and its Compact Fully Integrated Ka-band Implementation," Proc. IEEE International Microwave Symposium (IMS), Jun. 2018.

[22] M. Huang and H. Wang, "An Ultra-Compact Folded Inductor Based Mm-Wave Rat-Race Coupler in CMOS," Proc. IEEE International Microwave Symposium (IMS), May 2016.

[23] F. Erkmen, *et al.*, "Scalable electromagnetic energy harvesting using frequency-selective surfaces," *IEEE Trans. Microw. Theory Techn,* vol. 66, no. 5, pp. 2433–2441, May 2018

[24] Y. Hu, *et al.*, "Grid-Array Rectenna With Wide Angle Coverage for Effectively Harvesting RF Energy of Low Power Density," *IEEE Trans. Microw. Theory Techn*, pp. 1–12, Dec 2018